sustainability

MDPI

Review

Is K-Struvite Precipitation a Plausible Nutrient Recovery Method from Potassium-Containing Wastes?—A Review

Işık Kabdaşlı [1,*,†], Alessio Siciliano [2,*,†], Carlo Limonti [2,†] and Olcay Tünay [1,†]

[1] Environmental Engineering Department, Civil Engineering Faculty, İstanbul Technical University, Ayazağa Campus, Sarıyer, İstanbul 34469, Turkey
[2] Laboratory of Sanitary and Environmental Engineering, Department of Environmental Engineering, University of Calabria, 87036 Rende, CS, Italy
* Correspondence: kabdasli@itu.edu.tr (I.K.); alessio.siciliano@unical.it (A.S.)
† These authors contributed equally to this work.

Abstract: The definition of technologies capable of removing and recovering nutrients from polluting effluents is a key environmental challenge. Through these technologies, it would be possible to protect aquatic systems and prevent the consumption of natural resources for the production of commercial fertilizers. In this regard, the application of the precipitation processes of struvite-type compounds is an attractive approach. Indeed, these processes are potentially able to remove nutrients from many effluents and produce a precipitate reusable as a slow-release fertilizer. The scientific community has largely focused on the precipitation of magnesium ammonium phosphate ($MgNH_4PO_4 \cdot 6H_2O$, MAP), while the recovery of the analogous magnesium potassium phosphate ($MgKPO_4 \cdot 6H_2O$, MPP) has received extensive attention in the last decade. Research on this topic is continuously progressing to improve the precipitation process in different aspects (working conditions, reaction units, interference elimination, etc.). Until now, there has been no paper that comprehensively reviewed the applicability of MPP precipitation for the removal and recovery of nutrients from aqueous waste. To fill this gap, the present paper aimed to provide an exhaustive analysis of the literature reports on MPP processes to help researchers understand the theoretical and applicative aspects, the main problems, and the need for further research. In this regard, the applications in the treatment of various aqueous wastes were considered. The theoretical concepts, the main process parameters, and the effects of inhibiting substances and impurities are presented. Moreover, the development of reactor configurations and their working conditions are evaluated. Finally, the potential use of MPP as a fertilizer and some economic evaluations are reported. On the basis of the conducted analysis, it emerged that the recovery of MPP was mainly affected by the pH, dose, and nature of reagents, as well as the presence of competitive ions. The optimal pH values were reported to be between 9 and 11. Reagent overdoses with respect to the theoretical values improved the process and the use of pure reagents guaranteed superior performance. The stirred-tank reactors and fluidized bed reactors were the most used units with high process yields. The applicability of MPP in agronomic practices appears to be a suitable option.

Keywords: K-containing wastes; K-struvite precipitation; nutrients; potassium and phosphorous recovery

Citation: Kabdaşlı, I.; Siciliano, A.; Limonti, C.; Tünay, O. Is K-Struvite Precipitation a Plausible Nutrient Recovery Method from Potassium-Containing Wastes?—A Review. *Sustainability* **2022**, *14*, 11680. https://doi.org/10.3390/su141811680

Academic Editor: Hosam M. Saleh

Received: 8 August 2022
Accepted: 8 September 2022
Published: 17 September 2022

Publisher's Note: MDPI stays neutral with regard to jurisdictional claims in published maps and institutional affiliations.

Copyright: © 2022 by the authors. Licensee MDPI, Basel, Switzerland. This article is an open access article distributed under the terms and conditions of the Creative Commons Attribution (CC BY) license (https://creativecommons.org/licenses/by/4.0/).

1. Introduction

The discharge in the environment of waste and wastewater with high levels of nutrients is a matter of great concern. In fact, this practice induces negative consequences on the environment such as eutrophication phenomena. Numerous biological and physico-chemical treatments for the abatement of nutrients have been developed [1]. Among the many alternatives, a solution based on nutrient recovery and reuse is very advantageous because it promotes the development of sustainable technologies [1]. In

effect, the definition of a virtuous cycle of nutrients to reduce the use of natural resources while also avoiding pollution phenomena is currently a key challenge. In this context, magnesium ammonium phosphate ($MgNH_4PO_4 \cdot 6H_2O$; MAP) precipitation application began some 30 years ago and research in this area is still continuing [2–13]. The impetus behind these works was that the precipitate obtained from the treatment of waste is a valuable product containing two essential elements (nitrogen and phosphorus) that can be used as a slow-release fertilizer in agronomic practices [3,14]. The other benefits of the process are protection from environmental pollution, particularly prevention of eutrophication, and a contribution to sustainability through a lesser use of phosphate resources [1]. All the above considerations apply to the case of the precipitation of the analogous magnesium potassium phosphate ($MgKPO_4 \cdot 6H_2O$; MPP), which also produces a valuable substance with two fundamental elements (potassium and phosphate) for plant growth [15]. MPP precipitation is particularly advantageous because it is the only method to selectively remove, recover, and reuse potassium that has hitherto been supplied by natural resources in fertilizing activities [16].

The studies on MPP began in the 2000s [17,18] but have received extensive attention over the last decade.

The precipitation of MPP is characterized by a significant complexity in which the solubility product of MPP and inhibitory substances are among the most important factors. Indeed, while the solubility product of MAP (pK_{so}) was found to vary between 12.60 and 13.36 [19], the reported MPP solubility product values were between 10.77 and 12.22 [6,20–22], exhibiting an order-of-magnitude difference with MAP, which is of primary importance in determining precipitation efficiency. In addition, inhibiting substances, mainly ammonia and calcium, prevent the formation of MPP depending on their concentrations [16]. Particularly for ammonium, which has a high concentration in many wastes, it is important to determine a threshold concentration below which MPP can start to precipitate [14,23]. This point may also be used to decide if the ammonia and potassium components could be obtained separately or as a combination using coprecipitation of these two valuable products [14,23]. In some cases, pretreatments for ammonia removal are necessary to obtain effective potassium precipitation [19]. Sodium coprecipitates with MPP as magnesium sodium phosphate ($MgNaPO_4 \cdot 7H_2O$; MSP), while magnesium can induce the generation of some magnesium phosphates (amorphous magnesium phosphates and bobierrite ($Mg_3(PO_4)_2 \cdot 8H_2O$)) and magnesium hydroxide ($Mg(OH)_2$) [16]. The formation of these compounds causes a demand for additional phosphate doses and impairs the purity of the precipitate.

The problematic aspects of the process such as complex chemistry, effects of inhibitory substances, and the need to determine the optimum conditions for each type of wastewater has been largely facilitated using modeling studies [19,20,24]. Indeed, thermodynamic models allow a realistic assessment of the process application [19,20,24].

In a similar way to that of MAP, which has a great spectrum of applications from source-separated urine to slaughterhouse wastewaters [6], the tannery industry [25], etc., there are several wastes, including poultry wastes and semiconductor production wastewaters [26–28] for which MPP precipitation processes were tested.

The studies in the field also covered bench scale experiments [16], baffle reactors [29], fluidized bed reactors [30], and even electrochemical applications [13].

In some works, the costs of the process were calculated [31,32]. However, there are elements of the process economics that cannot be envisaged in a quantitative manner; sometimes these elements may override other expenses in terms of priority. These are: resource protection and reuse, sustainability, and protection of the environment, which are all quite important in the case of MPP precipitation.

We found over 50 published papers and book chapters on the subject of MPP precipitation. The publications, which covered almost all aspects of the process, showed that the areas in which K-struvite precipitation is being applied are increasing. Currently, there is a lack of comprehensive reviews on the development of K-struvite recovery

processes. The purpose of the study was to assess the literature to determine: the level of research while paying attention to modeling studies as well as to substances that interfere with MPP precipitation, applications to all wastes that have been tested in the literature, practical aspects, reactor types, and operational problems. All these data were comparatively assessed, the gaps in the information were pointed out, and the need for further studies in the field and future perspectives were emphasized.

2. Chemical and Physical Characteristics of K-Struvite

2.1. Crystallographic Properties

Struvite-type compounds are characterized by the general formula $A^{2+}B^{+}PO_4^{3-}{\cdot}yH_2O$, where A^{2+} represents a bivalent cation such as (Mg^{2+}, Mn^{2+}, Ca^{2+}); B^{+} is a monovalent cation such as NH_4^{+}, Rb^{+}, Mn^{+}, K^{+}, Na^{+}, or Ti^{+}; and y = 6–8 [33–35]. Magnesium potassium phosphate ($MgKPO_4{\cdot}6H_2O$), or K-struvite, is one of the compounds in the struvite family; its structure is similar to those of other crystals. In particular, $MgKPO_4{\cdot}6H_2O$ is isostructural with ammonium struvite (MAP) [34]. K-struvite has a slightly greater density (1.864 g/cm^3) [36] than MAP (1.711 g/cm^3) [37]. The substitution of ammonium cation with potassium produces only minor structural crystal modifications because the ionic radius of K^{+} is analogous to that of NH_4^{+} [38].

Similar to struvite, the structure of K-struvite consists of PO_4^{3-} tetrahedra, $[Mg(H_2O)_6]^{2+}$ octahedra, and K^{+} groups connected by hydrogen bonds [34,37,39]. Each K^{+} ion is bound to five O atoms, with one from the phosphate tetrahedra and four from the H_2O molecules [34]. The geometry of the K^{+} ion coordination can be represented as tetragonal pyramidal with the oxygen from PO_4^{3-} at the axial position and the water molecules at the base [34]. Figure 1 displays the crystal structure of K-struvite as reported by Graeser et al. [36]. The K-O bonds involving H_2O are quite weak due to the interatomic distance, which is at least 0.16 Å greater than the sum of the ionic radii [34]. The K-O bonds are much weaker than those of Mg-O, the distances of which change from 2.042 to 2.103 Å [34]. These values are very similar to those of ammonium struvite [34], so the substitution of NH_4^{+} with K^{+} into the structure does not significantly influence the Mg-O bonds. In effect, according to Mathew and Schroeder [34], the replacement of NH_4^{+} with K^{+} has a slight impact on the structure because the interactions between the larger cations and the O atoms are weak in struvite-type crystals.

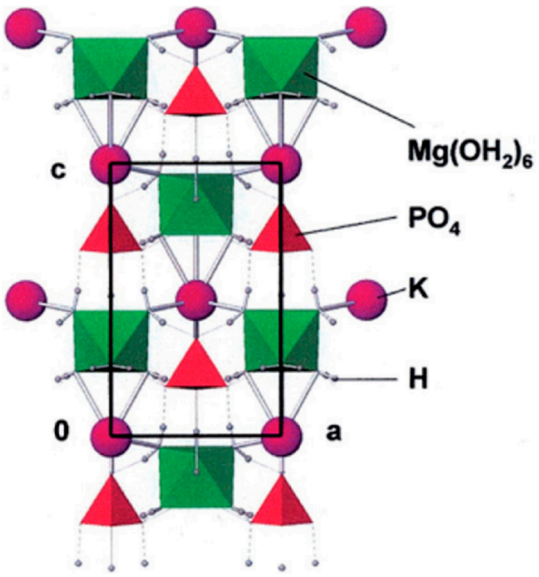

Figure 1. Crystal structure of K-struvite displaying the H-O bonds [36]. Reprinted/adapted with permission from the managing editor of the European Journal of Mineralogy.

K-struvite forms have an orthorhombic needle-like crystalline shape and a transparent to whitish appearance [17,36,39]. Scanning electron microscopy (SEM) and energy-dispersive X-ray spectroscopy (EDS) were often applied to observe and analyze the chemical composition of K-struvite crystals produced by different precipitation processes. Various morphologies were detected by changing the treated wastewater, the reactor configuration, and the precipitation conditions [21,38].

In the experiments conducted by Wilsenach et al. [17], crystals with the typical orthorhombic structure of K-struvite were produced by treating synthetic urine in a stirred-tank reactor with a compartment for liquid–solid separation. On the basis of SEM images of the precipitate recovered under different operating conditions, the authors noted that the optimization of the mixing modality and the limitation of supersaturation could favor an increase in crystal size [17]. In particular, noticeably thicker crystals could be obtained, which should have led to better compaction during the settling phase [17]. Despite this, the precipitate produced always had a very high struvite volume index [17].

SEM analysis of the precipitate from the electrochemical treatment of simulated urine at 1.0 and 5.0 $mA \cdot cm^{-2}$ using a sacrificial Mg anode showed some difference in response to the change in current density [13]. The precipitate recovered at 1.0 $mA \cdot cm^{-2}$ had finer rod-like crystals with few impurities on the surface. On the contrary, the rod-like product at 5.0 $mA \cdot cm^{-2}$ was longer and had more amorphous impurities attached to the crystals. EDS analysis revealed the presence of small amounts of $MgNaPO_4 \cdot 6H_2O$ and $Ca_3(PO_4)_2$ that increased with the current density [13].

With respect to the crystals generally produced from synthetic urine, those collected by Xu et al. [29] from real urine were much thinner [14,17], with average dimensions between 60 and 100 μm. The formation of smaller crystals was attributed to the higher supersaturation in real urine, which was confirmed to potentially affect crystal growth [40].

The CO_2-assisted phosphorus extraction from poultry litter with addition of EDTA permitted the production of typical MPP needle-like orthorhombic crystals free of calcium phosphates [28]. The increase in the precipitation pH from 8.5–9.0 to 10.5–11.0 caused the production of crystals with a greater aspect ratio, which grew from 2.9 (±0.62) to 5.5 (±1.7).

Siciliano et al. [31] recovered $MgKPO_4 \cdot 6H_2O$ with a high purity grade from agro-industrial waste after an integrated treatment of three technologies (anaerobic digestion, supercritical water gasification (SCWG), and nutrient recovery). The liquid phase from the SCWG was suitable for the recovery of phosphorus in the form of K-struvite because ammonia was removed during gasification. The precipitate recovered from the precipitation process conducted at pH = 10 and Mg/P = 1 analyzed using SEM showed the presence of crystals with the typical orthorhombic shape of pure magnesium potassium phosphate (Figure 2a) and the presence of Mg, K, and P (Figure 2b) in a molar ratio of about Mg:K:P = 1:1:1.03.

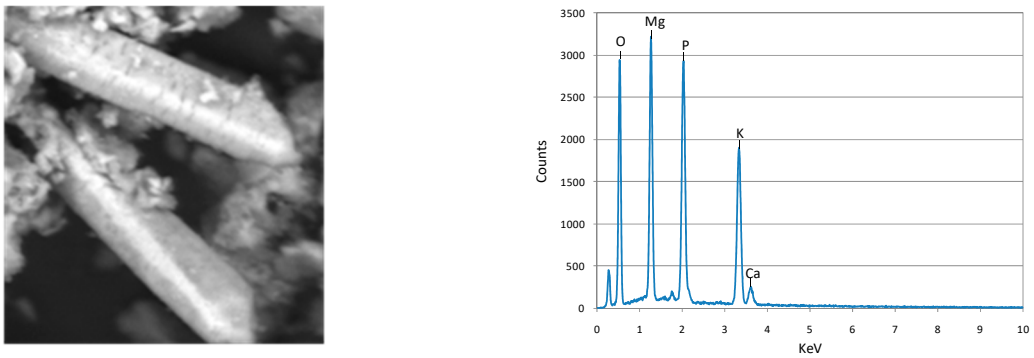

(**a**) (**b**)

Figure 2. SEM image (**a**) and EDS spectrum (**b**) of K-struvite recovered from a digestate subjected to supercritical water gasification (pH = 10, Mg:P = 1) [31].

In addition to SEM-EDS analysis, the X-ray diffraction technique (XRD) was also widely applied for the recognition and characterization of struvite-type crystalline compounds. An XRD diffractogram consists of information on the position and intensity of the peaks. The positions of the peaks allow the discovery of the crystal structure and symmetry of the contributing phase, while the intensities indicate the scattering from each plane and denote the sample crystallinity [39]. Figure 3 displays the standard X-ray diffractogram of K-struvite crystals elaborated by Xu et al. [14]. For comparison, the diffractogram of MAP is also shown [14]. As can be easily observed, the 2θ positions of the K-struvite peaks were analogous to those of MAP pattern, which confirmed that the ion replacement resulted in only minimal structural modifications. Graeser et al. [36] determined the cell dimensions of synthetic K-struvite and of crystals from dolomitic rocks discovered in Lengenbach (Switzerland) and from the galena mine in Rossblei (Austria) (Table 1). The data showed how the exchange of NH_4^+ by K^+ slightly reduced the cell volume and produced negligible impacts on the structure [36]. In the treatment of real wastewater, the similar diffractograms of MPP and MAP complicate the identification of the two crystals through the X-ray technique.

Some works used FT-IR spectroscopy to analyze and identify K-struvite crystals. This technique is a valid method for the recognition of water molecules such as H_2O of crystallization and its bond state in minerals [38]. FT-IR analyzes the vibrations of O–H and the absorption bands that occur at distinct frequencies depending on the cations bound to the O-H groups [38]. Table 2 reports the vibration bands summarized by Chauhan et al. [38]. The authors found four zones in the spectrum of K-struvite representing the absorption imputable to the H_2O of crystallization (Table 2). The values of *v1* and *v2* symmetric stretching vibrations of PO_4^{3-} units were discovered at 1023.5 and 421.8 cm^{-1}, respectively; the positions of the asymmetric stretching vibrations *v3* were between 1066.8 cm^{-1} and 1239.4 cm^{-1}, and the position of *v4* was 507.8 cm^{-1}. The band at 687.6 cm^{-1} represents the oxygen–metal bond. The band located at 894 cm^{-1} indicates the deformation of OH^- linked to Mg^{2+}. These results were in good agreement with those previously reported in the literature [41].

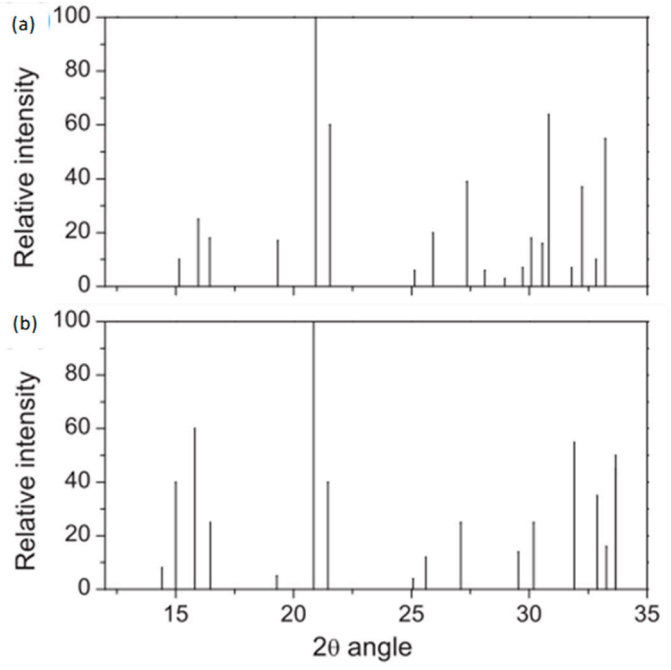

Figure 3. XRD diffractogram in the 2θ range 10–35 of the standard (**a**) $MgKPO_4{\cdot}6H_2O$ (Powder Diffraction File (PDF) No. 35-0812) and (**b**) $MgNH_4PO_4{\cdot}6H_2O$ (Powder Diffraction File, PDF No. 15-0762), [14]. Reprinted/adapted with permission from Elsevier.

Table 1. Unit-cell parameters of K-struvite crystals [36]. Reprinted/adapted with permission from the managing editor of the European Journal of Mineralogy.

	Space Group	a (Å)	b (Å)	c (Å)	V (Å)	Z
K-struvite (Lengenbach): from structure determination	$Pmn2_1$	6.892 (2)	6.166 (2)	11.139 (4)	473.4 (3)	2
K-struvite (Lengenbach): refined from XRD data	$Pmn2_1$	6.903 (3)	6.174 (2)	11.146 (3)	475.0 (2)	2
K-struvite (Rossblei). From XRD data	$Pmn2_1$	6.878 (1)	6.161 (1)	11.100 (1)	470.41 (9)	2
K-struvite (PDF#35-0812)	$Pmn2_1$	6.873	6.160	11.087	469.40	2
N-struvite (PDF#71-2089)	$Pmn2_1$	6.95	6.14	11.22	478.8	2

Table 2. Assignments of different absorption bands in the FT-IR spectrum of K-struvite [38]. Reprinted/adapted with permission from John Wiley and Sons.

	Assignments	Reported Infrared (IR) Frequency Wavenumbers (cm^{-1})	Observed IR Frequency Wavenumbers (cm^{-1})
Absorption peaks due to water of crystallization	H–O–H stretching vibrations of water crystallization	3280 to 3550	3276.7, 3389.9,3521.6
	H–O–H stretching vibrations of cluster of water molecules of crystallization	2060 to 2460	2375, 2480.5
	H–O–H bending modes of vibrations	1590 to 1650	1655.7, 1704.5
	Wagging modes of vibration of coordinated water	808	894
Absorption peaks due to PO_4 units	ν1 symmetric stretching vibration of PO_4 units	930 to 995	1023.5
	ν2 symmetric bending vibration of PO_4 units	404 to 470	421.8
	ν3 asymmetric stretching vibration of PO_4 units	1017 to 1163	1066.8, 1168.6, 1239.4
	ν4 asymmetric bending modes	509 to 554	507.8
Metal–oxygen bonds	Metal–oxygen bonds	400–650	687.6
	Deformation of OH linked to Mg	847	894

2.2. Thermodynamic Properties of K-Struvite

Thermal stability is an important characteristic for the application of K-struvite as a potential slow-release fertilizer. A thermogravimetric analysis of K-struvite was conducted by Chauhan et al. [38]. The results obtained by the authors showed that K-struvite began to dehydrate at approximately 75 °C, and finally at 600 °C it was reduced to 64.14% of the initial mass and remained substantially unchanged up to 900 °C. The main mass loss occurred at temperatures above 100 °C, which denoted the association of H_2O molecules with the K-struvite structure.

Zhang et al. [42] conducted dehydration tests at different heating rates (2–20 K/min) and found that the weight loss of synthesized K-struvite powder began at 60 °C and ended at 250 °C, with a residual mass of about 58.5% regardless of the applied heating rate. At a lower heating rate, a lower temperature of starting dehydration and a lower temperature of a wide mass-loss peak were observed.

Lothenbach et al. [22] detected the weight loss of K-struvite at a temperature slightly higher than 100 °C. The overall quantified mass loss was about 41.1%, which agreed with the theoretical value of 40.5 % for complete dehydration:

$$MgKPO_4{\cdot}6H_2O \rightleftarrows MgKPO_4 + 6H_2O$$

The thermogravimetric analysis of K-struvite conducted by Gardner et al. [43] confirmed the occurrence of a consistent mass loss (39.73%) up to a temperature of 200 °C. Through an in situ high-temperature XRD analysis of K-struvite, the authors discovered the existence of a crystalline–amorphous–crystalline transition between 30 and 350 °C [43]. Specifically, from 50 to 300 °C, K-struvite dehydration produced an amorphous

phase that was named δ-$MgKPO_4$. Recrystallization was observed at 350 °C that generated β-$MgKPO_4$. Further heating caused a subsequent transition to γ-$MgKPO_4$, which after cooling reversed to *α*-$MgKPO_4$, which was the structure stabilized at room temperature. This behavior indicated that K-struvite could potentially withstand high temperatures via a transition to $MgKPO_4$ and is different from struvite, in which NH_4^+ release occurs above 50 °C [43–45].

Luff and Reed [46] measured the low-temperature heat capacity (Cp) from 10 to 316 K and a value of about 324.8 J·(K·mole)$^{-1}$ was obtained at 25 °C. Similar values were detected in recent works [45]. The authors determined the standard enthalpy of formation (ΔH°) at 25 °C by considering the formation of MPP from the reaction of magnesium chloride and potassium dihydrogen phosphate and by assuming previous published values of the enthalpies of formation of KH_2PO_4, aqueous $MgCI_2$, and aqueous HCl. Using this approach, a value of −3722.06 kJ·mole^{-1} was obtained, which was comparable to the standard enthalpy of formation of −3718 ± 3 kJ·mole^{-1} determined by Lelet et al. [45] and the values of 3717 kJ·mole^{-1} and 3729 kJ·mole^{-1} estimated by Lothenbach et al. [22].

The standard molar entropy at 298.15 K was calculated from the data of Cp as a function of temperature [45]. A value of 352.7 ± 2.1 J·(K·mole)$^{-1}$ was obtained, which was in line with what was reported in other works [46]. Using the data of the measured standard entropy of K-struvite and those of elements of interest taken from the literature, the authors determined that the entropy of formation (ΔS°) was equal to −1576 ± 2 J·(K·mole)$^{-1}$ [45]. Finally, the standard molar Gibbs free energy of formation obtained using the values of ΔS° and ΔH° was −3248 ± 4 kJ·mole^{-1} [45].

The thermodynamic data published in the literature were applied to evaluate the fundamental parameters for the control of the crystallization process of K-struvite in aqueous solutions.

2.3. Solubility Product and Thermodynamic Modeling

The solubility product (K_{sp}) defines the equilibrium state of a solid dissolving into its constituent ions in a liquid. In the case of K-struvite, we have:

$$MgKPO_4 \cdot 6H_2O_{(S)} \rightleftarrows Mg^{2+} + K^+ + PO_4^{3-} \quad (1)$$

$$K_{sp} = [Mg^{2+}] \cdot [K^+] \cdot [PO_4^{3-}] \quad (2)$$

The previous equation shows that if the product of concentrations of Mg^{2+}, K^+, and PO_4^{3-} is higher than the K_{sp}, the solution is supersaturated and precipitation of K-struvite will occur. The K_{sp} value does not depend on other parameters such as pH and only changes with temperature. The K_{sp} is related to the Gibbs free energy (ΔG°) via the isotherm equation:

$$\Delta G° = -R \cdot T \cdot \ln K_{sp} \quad (3)$$

Considering the general formula of ΔG°:

$$\Delta G° = \Delta H° - T \cdot \Delta S° \quad (4)$$

Combining the two previous expressions:

$$\ln K_{sp} = -\frac{\Delta H°}{R \cdot T} + \frac{\Delta S°}{R} \quad (5)$$

The differentiation of this equation with respect to the variable T and by assuming that both ΔH° and ΔS° are independent from temperature leads to the van 't Hoff equation [47]:

$$\frac{d(\ln K_{sp})}{dt} = \frac{\Delta H°}{RT^2} \rightarrow \ln \frac{K_2}{K_1} = -\frac{\Delta H°}{R}\left(\frac{1}{T_2} - \frac{1}{T_1}\right) \quad (6)$$

A value of K_{sp} equal to $2.1 \cdot 10^{-12}$ (pK_{sp} = 11.67) was calculated by Luff and Reed [46] based on the thermodynamic data and using the equations reported above. However, as

a thermodynamic parameter, K_{sp} is hardly applicable in the case of real wastewaters due to the effects of several dissolved species other than the K-struvite constituents that reduce the precipitation potential of K-struvite [48]. For real liquors, a more effective method to assess saturation is in the form of the activity solubility product (K_{so}), which considers the overall ionic strength (I) and the activity (a) of the ionic species [48]. For K-struvite, K_{so} can be obtained by means of the following expression [45]:

$$K_{so} = a_{Mg^{2+}} \cdot a_{K^+} \cdot a_{PO_4^{3-}} \quad (7)$$

where $a_{Mg^{2+}}$, a_{K^+}, and $a_{PO_4^{3-}}$ are the activities of MPP elements. These parameters are defined as $a_{Mg^{2+}} = \gamma_{Mg^{2+}} \cdot [Mg^{2+}]$, $a_{K^+} = \gamma_{K^+} \cdot [K^+]$, and $a_{PO_4^{3-}} = \gamma_{PO_4^{3-}} \cdot [PO_4^{3-}]$, in which $\gamma_{Mg^{2+}}$, γ_{K^+}, and $\gamma_{PO_4^{3-}}$ are the activity coefficients and $[Mg^{2+}]$, $[K^+]$, and $[PO_4^{3-}]$ are the respective molar concentrations in the solution.

The values of K_{sp} and K_{so} coincide in the case of infinite diluted solutions ($\gamma_i = 1$). Such a condition occurs in practice for concentrations of the ionic species up to 10^{-3} mol·L^{-1} [49]. For real effluents, the ionic activities are instead influenced by the ionic strength:

$$I = \frac{1}{2}\sum_i [C_i] \cdot z_i^2 \quad (8)$$

where $[C_i]$ is the molar concentration of the species i and z_i is its electric charge. The relationship between the ionic activity coefficient γ_i and the ionic strength I is commonly defined by extended forms of the Debye–Hückel expression. According to the Davies' expression, γ_i can be estimated as follows:

$$-\log \gamma_i = A \cdot z_i^2 \left(\left(\frac{\sqrt{I}}{1+\sqrt{I}} \right) - B \cdot I \right) \quad (9)$$

where A is the Debye–Hückel parameter equal to 0.509 at 25 °C and B is 0.3 [19,20]. This equation is applicable up to an ionic strength of 0.5 M in the urine precipitation system [19].

The actual potential for crystal formation in a solution can be assessed using the supersaturation ratio (S) [48], which is defined as the ratio between the ionic activity product of the constituent ions of the substance and the activity solubility product (K_{so}):

$$S = \frac{a_{Mg^{2+}} \cdot a_{K^+} \cdot a_{PO_4^{3-}}}{K_{so}} \quad (10)$$

In effect, the supersaturation ratio is an expression of the driving force of crystallization [48]. When S < 1, precipitation is thermodynamically impossible; if S = 1, the system is at equilibrium; if S > 1, the solution is oversaturated and precipitation can occur.

Snoeyink and Jenkins [47] also presented the concept of the conditional solubility product (C_{sp}):

$$C_{sp} = C_{T,Mg^{2+}} \cdot C_{T,K^+} \cdot C_{T,PO_4^{3-}} \quad (11)$$

In which $C_{T,Mg^{2+}} = [Mg^{2+}]/\alpha_{Mg^{2+}}$, $C_{T,K^+} = [K^+]/\alpha_{K^+}$, and $C_{T,PO_4^{3-}} = [PO_4^{3-}]/\alpha_{PO_4^{3-}}$ are the total analytical concentrations, with $\alpha_{Mg^{2+}}$, α_{K^+}, and $\alpha_{PO_4^{3-}}$ representing the ionization fractions that can contribute to generate K-struvite. The C_{sp} can also be expressed as follows:

$$C_{sp} = \frac{K_{so}}{\left(\alpha_{Mg^{2+}} \cdot \alpha_{K^+} \cdot \alpha_{PO_4^{3-}}\right)\left(\gamma_{Mg^{2+}} \cdot \gamma_{K^+} \cdot \gamma_{PO_4^{3-}}\right)} = \frac{K_{sp}}{\left(\alpha_{Mg^{2+}} \cdot \alpha_{K^+} \cdot \alpha_{PO_4^{3-}}\right)} \quad (12)$$

The value of C_{sp} is pH-dependent; the minimum occurs when the product $\alpha_{Mg^{2+}} \cdot \alpha_{K^+} \cdot \alpha_{PO_4^{3-}}$ is at maximum [48]. This minimum value also corresponds to a pH minimum that is usually called the pH of minimum solubility [48] in the literature.

The ionic activities, the solubility products, and the saturation conditions can be estimated by considering a series of chemical reactions relevant to the studied system.

Iterative calculations are generally applied through the use of modeling software based on the thermodynamic chemical equilibrium [48]. Bennett et al. [21] calculated a K_{so} that gave the most accurate matching between the theoretical concentrations and the experimental values using theoretical concentrations that were generated by means of PHREEQC software. The estimated activity products (pK_{so}) were in the range of 11.07 ± 0.006–10.895 ± 0.007 for a temperature between 10 and 35 °C. The authors proved that the formation of K-struvite from synthetic wastewater can occur when the supersaturation ratio is greater than 1 and higher than the supersaturation ratios of other magnesium phosphates (such as cattiite), while a pure product can be formed at very high supersaturation.

Xu et al. [19], by means of thermodynamic modeling on PHREEQC software based on precipitation equilibrium at 25 °C, determined a pK_{so} equal to 12.22 ± 0.253 for K-struvite in synthetic urine.

Yang et al. [20] applied a model based on a series of identified reactions and equilibrium constants at 25 °C taken from the literature as well as on the Gibbs free energy of each component provided or obtained by calculation. The model consisted of three steps. The first step involved the initialization of I, ion concentrations, etc.; the Gibbs free energy for the system was used as the objective function to be minimized. The second step concerned the resolution of the system; a scalar function was considered as the objective function to be minimized. Finally, the activity solubility product of K-struvite was determined by extrapolating the calculated data to zero ionic strength. A pK_{so} of 10.872 was calculated at 25 °C [20].

Thermodynamic modeling was carried out by Lothenbach et al. [22] using the Gibbs free-energy-minimization program GEMS; a pK_{so} value equal to 10.77 ± 0.55 at 20 °C was calculated.

The differences among the values of the solubility product reported in the literature, were attributable to the different thermodynamic models, objective function, and solution methods applied [22].

In addition, the estimated values of the solubility product of K-struvite were quite lower than those summarized for MAP (12.60 to 13.36) [19]. This meant that struvite has a higher tendency to form than K-struvite, confirming that NH_4^+ in wastewater should be removed to allow MPP precipitation. This agreed with the thermodynamic calculations executed by Barat et al. [49] on supernatants of anaerobically digested sludge, according to which K-struvite was unlikely to precipitate.

3. Parameters Affecting K-Struvite Precipitation Performance

3.1. Operation pH

Operation pH affects MPP precipitation in various ways, such as in K^+ removal efficiency; coprecipitation of other compounds; interaction with and inhibition by foreign and/or hazardous substances, therefore affecting the purity and safety of the final product; crystallization; and crystal growth processes, mostly through a supersaturation mechanism. An accurate evaluation of these effects can best be made through thermodynamic modeling, as previously described. As will be dealt with in this paper, although there were several attempts in this area [19–22,50], it seems there is still a lack of information due to the complexity of the system under consideration. The problem of the complexity originates mostly from the number of solid phases and their precipitation–transformation–dissolution processes, which are mainly dependent on pH. On the basis of precipitating solids, the process can be evaluated in two pH ranges: values (i) up to 9.0 and (ii) over 9.0. For the process realized under pH 9.0, a significant contribution to the subject came from K-struvite cement research, particularly the studies involving a high water (w) to cement (c) ratio (w/c of 100). This ratio was on a weight basis, where c was the total of ($MgO+KH_2PO_4$) in equal amounts. Chau et al. [51] conducted a cementation at 10 g solids per 100 mL water in which the solids contained Mg and K and the Mg/P ratios were 4–12.

The initial pH was approximately 7.5, which increased to 10.5 through the reaction. According to mineralization evaluations, phosphorrosslerite ($MgHPO_4{\cdot}7H_2O$) was the first phase and $Mg_2KH(PO_4)_2{\cdot}15H_2O$ was the second, which converted to $Mg_2KH(PO_4)_2{\cdot}15H_2O$ [48]. $Mg_2KH(PO_4)_2{\cdot}15H_2O$ was later MPP transformed to the stable phase of MPP [51]. Lahalle et al. [52] performed a similar experiment and found that within one hour and at pH 4, the K concentration in solution was unchanged while that of Mg and P decreased. This was interpreted by the authors as the formation of magnesium phosphate; the solid phase was newberyite ($MgHPO_4{\cdot}3H_2O$) rather than phosphorrosslerite. Between pH 4 and 8.5 for an additional 4 hours, $Mg_2KH(PO_4)_2$ precipitated and subsequently (after 8 h) transformed into MPP and cattiite (trimagnesium phosphate; $Mg_3(PO_4)_2{\cdot}22H_2O$). The final solution composition remained unchanged at the end of experiment (30 h), at which point the solution pH had been increased to 10. Le Rouzic et al. [53] found in a similar work conducted using a more concentrated solution that only two phases precipitated: newberyite in the acid phase and MPP in the alkali range. A further study of Lahalle et al. [54] again verified the precipitation sequence of phases: newberyite, $Mg_2KH(PO_4)_2$, MPP, and cattiite. They also emphasized that newberyite was a degradation phase of phosphorrosslerite. Lothenbach et al. [22] carried out a detailed study to determine the compounds and their thermodynamic constants for the same system. They found the existence of additional magnesium phosphate compounds such as $Mg_3(PO_4)_2{\cdot}4H_2O$ and bobierrite ($Mg_3(PO_4)_2{\cdot}8H_2O$). Phosphorrosslerite was defined as an intermediate compound that was converted to newberyite with time. For pH 7–8, $Mg_2KH(PO_4)_2$ and $Mg_3(PO_4)_2{\cdot}22H_2O$ were found to be stable, while above pH 8, MPP was stable but only for a high K concentration exceeding 30 mM. The water/solute and Mg/P ratios were also noted as parameters that determined the solution composition. Yang et al. [20] also pointed out that MPP and cattiite precipitated together at a much greater w/c ratio of 100. So, while these studies defined mainlines, there seems to be a need for further research to elaborate the stability and composition of precipitating compounds, particularly for magnesium phosphates. The same applies to the second pH range beginning with 9, which is the main area of MPP precipitation for K and P recovery. In fact, this range can be narrowed to pH 9–12. In their experimental study using synthetically prepared urine (SPU) and a Mg:K:P molar ratio of 1.6:1:1.6, Xu et al. [14] found that K removal performance decreased with pH, as will be detailed in Section 4.1. The reason for this loss in efficiency was likely brucite ($Mg(OH)_2$) precipitation, which became competitive at high hydroxide concentrations. Magnesium phosphate precipitation could be another reason. Both mechanisms reduced the magnesium concentrations available for MPP precipitation. Xu et al. [19] created a thermodynamic model of MPP precipitation using data obtained from experiments on SPU. Their model outputs also pointed out a significant drop in K recovery efficiency above pH 11. Harada et al. [55] found that in MPP precipitation, K removal efficiency was reduced as the pH was increased from 11 to 12. In their experimental study of MPP precipitation with diluted manure, Tarragò et al. [56] reported magnesium hydroxide precipitation after pH 10.5. Therefore, except for a few, all the MPP precipitation studies we found were conducted between pH 9 and 11.5. Basically, the effect of pH on MPP precipitation can be evaluated using Equation (13), as suggested by Wilsenach et al. [17] for pH values around 10:

$$Mg^{2+} + K^{+} + HPO_4^{2-} + 6H_2O \rightleftarrows MgKPO_4{\cdot}6H_2O + H^{+} \quad (13)$$

However, as the pH was increased above 11, the phosphate equilibrium shifted from HPO_4^{2-} to PO_4^{3-}, forming MPP but not producing the proton [19,23].

For MPP precipitation in any wastewater that contains (or has added) sodium but does not bear interfering ions such as ammonium and calcium, only three solid phases precipitate. These are MPP, MSP, and magnesium phosphates. As will be discussed in the following subsection, MSP always coprecipitates with MPP in the pH range of 9–11.5. Magnesium phosphates are another group of compounds that may precipitate together with MPP. Within this group are: bobierrite (pK_{so} = 25.2; precipitation pH range 8–10),

cattiite (precipitation pH range > 9), and newberyite (precipitation pH range < 6) [57]. There is also amorphous magnesium phosphate ($Mg_3PO_4 \cdot xH_2O$). Newberyite did not precipitate under the conditions of MPP precipitation, while others aimed to convert to the stable-phase bobierrite. Taylor et al. [58] defined a stability condition when MAP and cattiite solids were present. Cattiite was also considered to be unstable at a low pH [59] because the conversion of phases in reaction kinetics is of importance. Warmadewanthi and Liu [57] assumed a slow reaction kinetics for cattiite based on the work of Mamais et al. [60]. This approach was adopted by researchers through the modeling of MAP and MPP precipitations; cattiite was excluded from the modeling in some studies [61–64]. However, both precipitates were experimentally found in the works of Yang et al. [20] and Lothenbach et al. [22]. In their experimental study, Tarragò et al. [56] found that the saturation index for MPP and magnesium phosphate (MP) increased up to pH 11.5 and then stabilized near pH 12. They also concluded that when the Mg/P molar ratio was higher than 2, MP was formed at a pH higher than 9.5. In their experimental study, Gao et al. [26] reported that as the MP formation at a Mg:K:P molar ratio of 1:1:1 and pH 8–10 significantly inhibited MPP precipitation. Warmadewanthi and Liu [57] experimentally found that bobierrite had mixed with amorphous magnesium phosphate based on XRD results showing bobierrite characteristic peaks at the maximum intensity at pH 10. Taylor et al. [58] demonstrated that bobierrite and trimagnesium phosphate coprecipitated together with MPP between pH 10.42 and 10.82. Wang et al. [65] included bobierrite in their MAP precipitation modeling study. Yang et al. [20] studied MPP precipitation experimentally and established a thermodynamic model. They proposed a solubility product for MPP and experimentally proved that MPP and cattiite precipitated together in a pH range of 10.5–12.5 and that the amount of cattiite increased as the pH rose from 10.5 to 11.5. The pH range of 10.5–11.0 covered in their study was very close to the range of 10.42–10.87 used by Taylor et al. [58] and was in accordance with their conclusion that cattiite was formed as a result of MPP dissolution and then transformed into bobierrite, although the solution may remain oversaturated with bobierrite. Bennett et al. [21] also conducted a theoretical and experimental study to determine the solubility product for MPP. In their work, it was found that to obtain pure MPP, a minimum K:P ratio of 45–50:1 was necessary to increase the supersaturation ratio of MPP relative to that of cattiite; to obtain pure MPP at pH 8, a phosphate concentration of 8 mM and a Mg:P ratio of 3:1 was required. They also found evidence of bobierrite precipitation. Huang et al. [59], who performed a study to recover phosphate from swine wastewater through MPP precipitation, determined that the optimum pH was 10 and indicated that MP precipitation rapidly increased as the pH rose from 8 to 10.5. In their study with SPU, Xu et al. [19] noted that amorphous MP precipitated below pH 8 or when the Mg:P molar ratio was 1:4. In chemical precipitation applications the aim is to separate a solid phase. The efficiency of precipitation increases as the solid phase is settled out. However, in practice, solid particles may be very small and/or their growth rate may be low that they cannot be separated out and remain in the solution. The extent of equilibrium is determined by solid species and their amounts is independent of whether the solids are in the solution or they are separated out. On the other hand, the solids that remain in the solution, often called fines, are lost in the solution and decrease the overall efficiency of the system. The phosphate and potassium losses through the effluent have been emphasized in the literature for MAP and MPP precipitations [66,67]. The above literature data indicated that MP precipitation was effective together with MSP for the equilibrium and MPP removal efficiency. Therefore, further studies will be useful to enlighten the role of MPs in MPP precipitation.

Table S1 presents the selected optimum pH values for MPP precipitation as applied to various waste streams. As seen in the table, all of the optimum pH values were within the range of 9–10.5 and were mostly around 10. Siciliano et al. [31] used a pH of 10 and a Mg:P molar ratio of 1:1 for MPP precipitation using a waste from agro industries. Xu et al. [19] selected pH 10.5 as an optimum and worked with Mg:P molar ratios ranging from 0.6 to 1.6. Le et al. [30] found that K recovery efficiency decreased after pH 10.5 and used this

value as the optimum. They also applied a Mg:P molar ratio of 2 and claimed that above this ratio, magnesium phosphate solids precipitated. Xu et al. [14] reported the optimum pH of the process as 10, emphasizing that there was a slight difference between pH 10 and 11 in terms of K removal efficiency. They also used a Mg:K:P molar ratio of 2:1:2. Kabdaşlı et al. [16] proposed a pH of 10 as the optimum for the same molar ratio as that of Xu et al. [14]. All of the above works were conducted on SPS and their conclusions were accordance with one another. However, as seen in Table S1, there were other wastes to which MPP precipitation was applied, and their optimum pH values were within the range of 10–11.

An over-stoichiometric dose is another key parameter for the process. An over-stoichiometric dose is applied to either to create a supersaturation for the compound to be precipitated or to compensate for another solid phase that has a common ion with the target solid phase. The excess doses should therefore be decided based on the advantages and disadvantages. The same applies to optimum pH determination. The only base that can be used as a pH adjustment agent in MPP precipitation is NaOH, which is expensive, and Na^+ precipitates out phosphate but not potassium. On the other hand, every high pH application leaves behind a solution in need of neutralization. MPP precipitation is an expensive process. A significant part of the cost is due to the chemicals that are used. It is a process with a valuable product; however, every process should be sustainable. The design and operation of chemical treatment is a complex task, particularly for the systems in which more than one solid is precipitated. The best approach is to have accurate thermodynamic models that can be used to analyze the above-mentioned decisions.

3.2. Magnesium and Phosphate Sources

The use of magnesium and/or phosphate is necessary for nutrient recovery in MAP and MPP precipitations due to their low amounts with respect to stoichiometry in most wastewaters [3,68]. The choice of these chemicals is of great importance because it is directly related to several operation parameters such as mixing conditions, operation time, and pH adjustment requirements [1,3]. The chemicals also play a determining role in the process efficiency, purity of MPP crystals, and effluent quality [3]. Although comprehensive reviews have focused on these chemicals, magnesium sources for MAP precipitation in particular were already available in the literature [1,3,68–70], and until now, very limited data have been published for MPP precipitation [13,32,71].

For MAP precipitation, chemical additions, namely a magnesium source, a phosphate source, and pH adjustment chemicals are important not only in terms of process efficiency and purity of the product, but also in terms of economic concerns. Few alternatives to phosphate addition have been identified [72,73]; generally sodium phosphates are used for this purpose. For pH adjustment, which is used mainly to increase the pH, several bases have been employed. Based on their effectiveness, these bases can be given in the order of KOH > NaOH > K_2CO_3 > Na_2CO_3. MgO, $Mg(OH)_2$, and $MgCO_3$ can also be utilized as both a magnesium source and a pH adjustment agent. Magnesium sources in the order of phosphate removal efficiencies can be given as $MgCl_2$ > $MgSO_4$ > MgO > $Mg(OH)_2$ > $MgCO_3$. Some of these compounds, such as $MgCl_2$, can be introduced to the solution directly, while some magnesium salts, particularly those with low solubility, can be fed into the solution after a pretreatment to increase their reactivity, such as dissolving in an acid solution. Together with their base-addition role in the cost of the process, cheaper alternatives such as seawater and bittern have been tested [1]. In addition, a number of natural-matter industrial byproducts, including wastes such as fly ash and wood ash, have been tested as potential sources of magnesium.

For MPP precipitation among the above-mentioned magnesium sources, $MgCl_2 \cdot H_2O$ is the most preferred salt in scientific research due to its high effectiveness [14,16,19,30,32,71,74] (Table S1). $Mg(OH)_2$ [32] and low-grade MgO (LG-MO) [71] were the alkali magnesium sources that had their efficiencies compared with $MgCl_2$. In some studies, the performance of K-struvite electro-precipitation with magnesium sacrificial anodes was also tested [13,32]. Sodium phosphate salts, particularly Na_2HPO_4, are the

most commonly used phosphate salts together with $MgCl_2$ (Table S1). The combination of these salts requires the addition of an alkali agent such as NaOH to elevate the solution pH. In some studies, a combination of an alkali magnesium salt such as $Mg(OH)_2$ and LG-MgO with H_3PO_4 was preferred to alleviate the sodium effect [32,71].

Huang et al. [32,71] realized comparative studies to determine the most efficient magnesium source to be used for K-struvite precipitation. For this purpose, the performance of $MgCl_2$, $Mg(OH)_2$, and a Mg sacrificial anode were experimentally compared in a study by Huang et al. [32]. As will be discussed in Section 4.1, their experimental data proved that $MgCl_2$ was the best magnesium source for the K-struvite precipitation, followed by the Mg sacrificial electrode and $Mg(OH)_2$ in terms of K recovery efficiency. In a study by Shan et al. [13], an electrolysis application performed at an optimum current density of 3.5 mA cm^{-2} and a K/P of 1:0.6 yielded lower K (35.4%) and P (88.5%) recovery efficiencies than those of Huang et al. [32]. It is worth emphasizing that the current density (7.5–17.5 $mA \cdot cm^{-2}$) applied by Huang et al. [32] was much higher than 3.5 $mA \cdot cm^{-2}$.

Another study by Huang et al. [71] focused on the usability of LG-MO in K-struvite precipitation. LG-MO derived from the calcination of magnesite mineral was used in three combinations: (i) alone (M1), (ii) together with H_3PO_4 (M2), and (iii) as a stabilizing agent (SA) preformed by H_3PO_4 (M3). The use of LG-MO together with H_3PO_4 or after precipitation with H_3PO_4 to produce SA yielded high K recovery efficiencies (70%) ; the lowest K recovery efficiency was obtained in the case of LG-MO alone. In the cases of M1 and M2, the phosphorous was completely recovered, whereas phosphorous recovery efficiency was decreased due to the dissolution of P in the presence of SA.

Our literature survey indicated that the published data for K-struvite were limited to a few scientific works, so further research is required to find cheaper and easy-to-use alternative precipitating agents with a higher reactivity while bearing a low level of impurities.

3.3. Presence of Competitive Ions

3.3.1. Ammonia

Ammonia is the main competitive ion for MPP precipitation due to the much lower solubility of MAP, which precipitates at or close to the pH region of that of MPP [19]. Since source-separated human urine is an important target of MPP precipitation and some other wastes such as anaerobic digestate contain ammonia, pretreatment of ammonia before MPP precipitation or coprecipitation of MAP and MPP has been a subject of scientific studies [29,30,75]. Some of the studies aimed to find a limit for ammonia for minimum interference with MPP precipitation. By using thermodynamic modeling developed for MPP precipitation for the SPU, Xu et al. [19] predicted that at pH 9 and a Mg:P molar ratio of 1, MPP would begin at as low as 50 mM of ammonia. Le et al. [30] conducted jar-test experiments on the SPU by adding ammonia at 0–800 $mgN \cdot L^{-1}$ at pH 10 and a Mg:P ratio of 1.5. The experimental results showed that the potassium removal sharply decreased from 61% to 15% as the ammonium concentration reached 800 $mgN \cdot L^{-1}$. On the other hand, almost the same P removal efficiencies (~97%) were obtained, indicating the precipitation of MAP and the formation of amorphous solids such as $Mg_3(PO_4)_2$ and $Ca_3(PO_4)$. As will be detailed in Section 4.1, Xu et al. [14] reported that the presence of ammonia yielded low K removal efficiencies as a consequence of coprecipitation of MAP and MPP. Gao et al. [23] studied the effects of ammonia on MPP precipitation using the SPU and found that at pH 11 and when using a Mg:K:P ratio of 1:1:1, as the ammonia concentration was elevated from 0 to 30 mM, the K removal efficiency decreased from 56% to 1%. Huang et al. [59] applied coprecipitation of MAP and MPP using an SPS containing approximately 400 $mgN \cdot L^{-1}$ of ammonia, 200 mg L^{-1} of potassium, and 40 $mg \cdot L^{-1}$ of calcium at pH 9.5 and a Mg:P ratio of 1:1. As expected due to the composition of the solution and the operation pH, MPP did not precipitate until a huge amount of potassium was added. In contrast with these findings, Harada et al. [55] reported that MPP precipitation

performance was not affected by the presence of ammonia based on their experimental data obtained for a SPS with initial concentrations of 2.56 mM K, 6.5 mM PO_4-P, and 5.6 mM NH_3-N.

As seen in the summary of the relevant literature, the studies in this area were far from satisfactory. As mentioned at the beginning of this review, a majority of the potential wastes to be considered as a source of potassium contain ammonium, and there is no method available to provide complete ammonia removal. Therefore, there is a need for further research on MAP and MPP coprecipitation.

3.3.2. Calcium

Calcium phosphates have a complex chemistry [76]. In fact, all calcium phosphates ultimately convert to the most thermodynamically stable hydroxyapatite ($Ca_5(PO_4)_3OH$); HAP) through a number of intermediate calcium phosphate solids, which, in the order of decreasing solubility, are: tricalcium phosphate ($Ca_3(PO_4)_2$; whitlockite; TCP), octacalcium phosphate ($Ca_8H_2(PO_4)_6 \cdot 5H_2O$; OCP), dicalcium phosphate ($CaHPO_4$; monetite, DCP), and dicalcium phosphate dehydrate ($CaHPO_4 \cdot 2H_2O$; brushite DCPD). In addition, amorphous calcium phosphate ($Ca_3(PO_4)_2 \cdot nH_2O$; ACP), which has no crystalline structure as one of the many precursors, exists. ACP is important because it is an initial phase. ACP first transforms into OCP and then into stable-phase HAP between pH 7 and 9. At pH values higher than 9, ACP transforms to HAP without an intermediate step [39]. However, the HAP amount decreases particularly after pH 10. This decrease was explained by the precipitation of other calcium phosphates. The presence of magnesium is also important due to its inhibitory effect [77].

Magnesium phosphate, as explained above, makes the picture even more complex. In addition to solution pH, alkalinity and the presence of other crystal inhibitors such as organic matter are among the parameters that affect calcium phosphate precipitation [63,77–81]. Magnesium, the common ion of MAP and MPP, plays an important role in calcium phosphate precipitation. Magnesium acts as an inhibitor of the conversion of ACP to the stable HAP. This conversion is not possible for Mg/Ca molar ratios greater than 4 [63,64]. The effect of magnesium is attributed to the incorporation of magnesium ions into HAP and prevention of the growth of prenuclei. For this effect, the Mg/Ca ratio is considered to be more related to the process than the magnesium concentration [79,80]. Calcium phosphate precipitation has been found in some of MAP precipitation studies. Li et al. [81] included monetite in their model. In their MAP precipitation, Lee et al. [75] took HAP, ACPs, TCP, and OCP into account as the precipitating solids. Çelen et al. [61] also considered DCP and DCPD in their MAP precipitation model. In their MAP precipitation modeling discussion, Lee et al. [24] concluded that calcium phosphate precipitation should be included in the models and also noted that the presence of calcium with a Ca/Mg ratio > 0.5 can lead to competitive calcium phosphate precipitation, which can cause scaling on the equipment. The magnesium/calcium ratio is also used to compensate for the negative effect of calcium: a Mg/Ca ratio over 2 was found to offset the calcium effect in MAP precipitation, while a ratio below 0.2 affected HAP nucleation [68]. It was also experimentally proved that ACP coprecipitating with MAP completely dissolved at a Mg/Ca ratio > 1.5 [82]. The presence of calcium resulted in a decrease in MAP crystal sizes [80,83,84].

3.3.3. Sodium

Magnesium sodium phosphate (MSP) is a struvite family member and has a comparable solubility product with that of MPP [19]. As such, it is an inevitable interfering precipitate together with MPP precipitation. Sodium ions are abundant in urine. Other wastes such as anaerobic sludge digestate contain sodium ions. Even if there is no sodium in the wastes being treated, sodium is introduced into the system as sodium hydroxide for pH adjustment in the MPP precipitation process. Therefore, MSP and its characteristics and the effects on MPP precipitation should be well evaluated. Mathew et al. [35] introduced MSP as a new member of the struvite family. Greaser et al. [36] found the MSP mineral in

nature. Chauhan et al. [38] obtained an MSP crystal using single-diffusion gel techniques. Yang and Sun [85] determined a $Mg_2KNa(PO_4)_2{\cdot}14H_2O$ crystal that was similar to the MSP. Gardner et al. [43] and Lelet et al. [45] defined the structure and characteristics of MSP. Tansel et al. [86] stated that $MgNaPO_4{\cdot}7H_2O$ was unstable in a solid state due to the high solubility of sodium salts. When MSP is present together with MPP as a fertilizer, such an instability may result in the washing out of MSP-bound phosphate into deeper layers of the soil by rain or irrigation. Xu et al. [19] were the first to take account of MSP in an MPP precipitation study conducted on the SPU. They claimed that feasible pH values for MSP would be higher than for MPP due to its lower precipitation potential. In their experimental study, they found that for a Mg:P molar ratio of 0.6–1.4 and a pH range of 8.5–11.5, MPP and MSP were the dominating precipitates, and at pH 10.5 and a Mg:P ratio lower than 1, MSP precipitation was promoted. However, under these increasing conditions, the Mg:P ratio may have caused magnesium phosphate precipitation. On the other hand, precipitation of MSP did not occur for a Na:K ratio lower than 2.1. Increasing Na:K ratios caused coprecipitation of MPP and MSP. This coprecipitation continued up to a Na:K ratio of 5.2, beyond which MPP precipitation was totally inhibited.

Huang et al. [71] used an SPS to test sodium and potassium competition by adjusting the Na:K ratio with NaCl. Initially, the potassium concentration was 49.8 mM and the Mg:K:P ratio was 1.6:1:1.6. The sodium concentration was increased between Na:K to 5–30. At a Na:K ratio of 10:1, a pH change between 10 and 12 had no effect on competitiveness. At pH 11, however, as the Na:K ratio was increased from 5 to 30, K recovery efficiency was reduced from 81 to 59%. Gao et al. [23] also used an SPS with 30 mM of K at a Mg:K:P ratio of 1:1:1 to assess the effects of sodium ions. The sodium doses ranged from 0 to 250 mM. At 250 mM of sodium, K removal decreased from 50 to 38%. Huang et al. [65] also worked with an SPS, but added only magnesium (25 mM), potassium (Mg:P ratio of 1:1), and sodium at increasing amounts to vary the pH from 8.5 to 12.5. The sodium content in precipitates and phosphate removal increased with an increasing pH up to pH 12, then both parameters began to decline. As in the case of calcium, these experimental studies shed some light on MSP precipitation and at least were indicative of the presence of MSP beginning at pH 8.5; an excess sodium also negatively affected the potassium removal. The decrease in both sodium and phosphate above pH 12 in the work of Huang et al. [32] was attributed to magnesium hydroxide precipitation. However, further studies supported by thermodynamic modeling will provide a more precise and clearer picture of the role of MSP in MPP precipitation.

3.4. Reactor Type and Operational Conditions

The reactor type and its configuration are considered to be important parameters that influence the process performance. Depending on the reactor geometry and its design characteristics, some operational problems may occur through K-struvite precipitation. Fine crystal formation is the most frequently reported problem faced during precipitation applications. Generally, uncontrolled primary nucleation due to localized supersaturation promotes the formation of the fines with a poor settling character. Sometimes the attrition and breakage of MPP pellets formed during the operation create a similar settling problem. As the crystal size of these fines ranges between 60 and 100 μm, the formation of fine crystals results in unsatisfactory K and P recovery efficiencies due to poor solid–liquid separation [67]. Another problem faced during precipitation applications is the scaling/fouling that occurs on the reactor walls and downstream conduits due to poor mixing or suspension conditions. Therefore, the selection of the reactor type and optimization of its operational conditions are of importance in achieving large MPP crystal sizes with a good settling character that yield a higher process performance. Within this context, various types of reactors such as stirred-tank reactors (STRs) [17,23], fluidized bed reactors (FBRs) [30,67], a draft tube and baffle reactor (DTBR), [29,75] and a bubble column reactor with draft tube (BCRDT) [15,50] have been developed for MPP crystallization (Table S1).

STRs can be operated either continuously (CSTR) [17] or in batch mode (BSTR) [62]. In the study by Perwitasari et al. [62], K-struvite precipitation that was performed in the BSTR was optimized using the surface response methodology for input variables of temperature (30–40 °C), stirring rate (200–400 rpm), and citric acid concentration (1–20 mg L^{-1}) to obtain an optimum mass of K-struvite crystals. Their data indicated that all input variables affected the amount of K-struvite precipitated at the tested ranges. An increase in both the temperature and stirring rate promoted the formation of K-struvite crystals, while an increase in citric acid concentration inhibited the crystal growth.

Wilsenach et al. [17] designed a CSTR with a specific liquid/solid separator to overcome the scaling problem observed in downstream conduits and to improve the settling characteristics of MAP or MPP crystals. The separator was constructed in two forms; namely, as inward and outward flow devices (Figure 4). A severe scaling problem occurred during all MAP experiments; at least 50% of the total volume of crystals attached to the CSTR wall, the impeller blades, and the outside of the internal effluent pipe, while a thin layer of crystals formed on the reactor wall during MPP precipitation experiments. This excessive scaling was explained by the localized superstations promoting primary nucleation instead of secondary crystal growth. The fine crystal problem observed in the effluent of the CSTR with an inward flow device was solved by using the outward flow device (depicted in the second reactor). To avoid the scaling and to produce crystals with a good settling character, the authors recommended that: (i) mixing and suspension of particles should be increased while the mixing speed is decreased to limit the centrifugal force and wall scaling; (ii) instead of primary nucleation, the secondary crystal growth must be promoted; (iii) diffuse dosing systems, rather than point dosing of reactants, can be used to prevent the localized supersaturation; and (iv) the above-mentioned operational problems can be handled by a reactor design based on computational fluid dynamics [17].

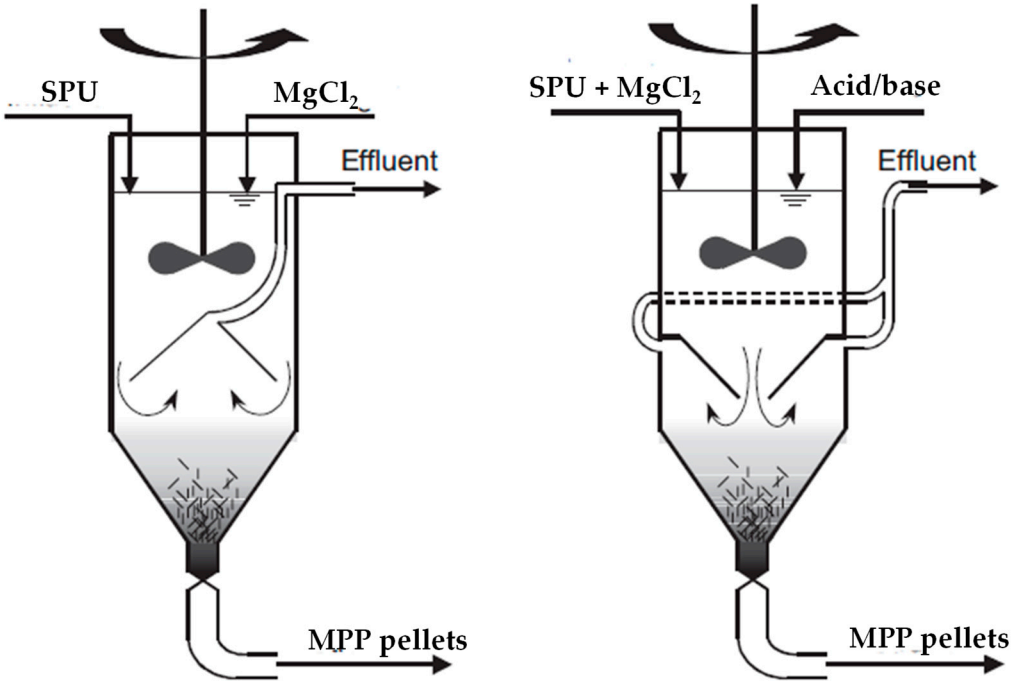

Figure 4. CSTR configurations used in the study by Wilsenach et al. [17]. Reprinted/adapted with permission from Elsevier.

Fluidized bed crystallization (FBC) is the most utilized recovery method applied to nutrient rich streams and wastes such as SSHU, swine waste, and manure [30,67]. This process is capable of recovering the N, P, and K as MAP or MPP pellets with a low water

content. The main advantages of the process are low chemical requirements and the usage of the produced pellets as a slow-release fertilizer for agricultural and gardening purposes [30]. The process also has some shortcomings in terms of seed requirements and a need for a high recirculation flow and up-flow velocity with a longer CRT [87]. Under moderate supersaturation conditions, the crystallization process in a FBR can be realized without using seeds. In this case, high-purity pellets were produced during the homogenous crystallization that took place in the FBHC column. Le et al. [30] used a FBHC column (schematized in Figure 5) for simultaneous P and K recoveries from the SPU. As will be explained in detail in Section 4.1, the operational parameters were optimized to attain the highest recovery efficiencies and to produce the pellets with the highest purity. The authors pointed out that the fluidization and up-flow velocities had a significant effect on the process performance. The minimum fluidization velocity (Umf) and optimum up-flow velocity of the FBHC process were determined to be 14.98 $m \cdot h^{-1}$ and 25–35 $m \cdot h^{-1}$, respectively, to maximize the K and P recovery in their experimental conditions.

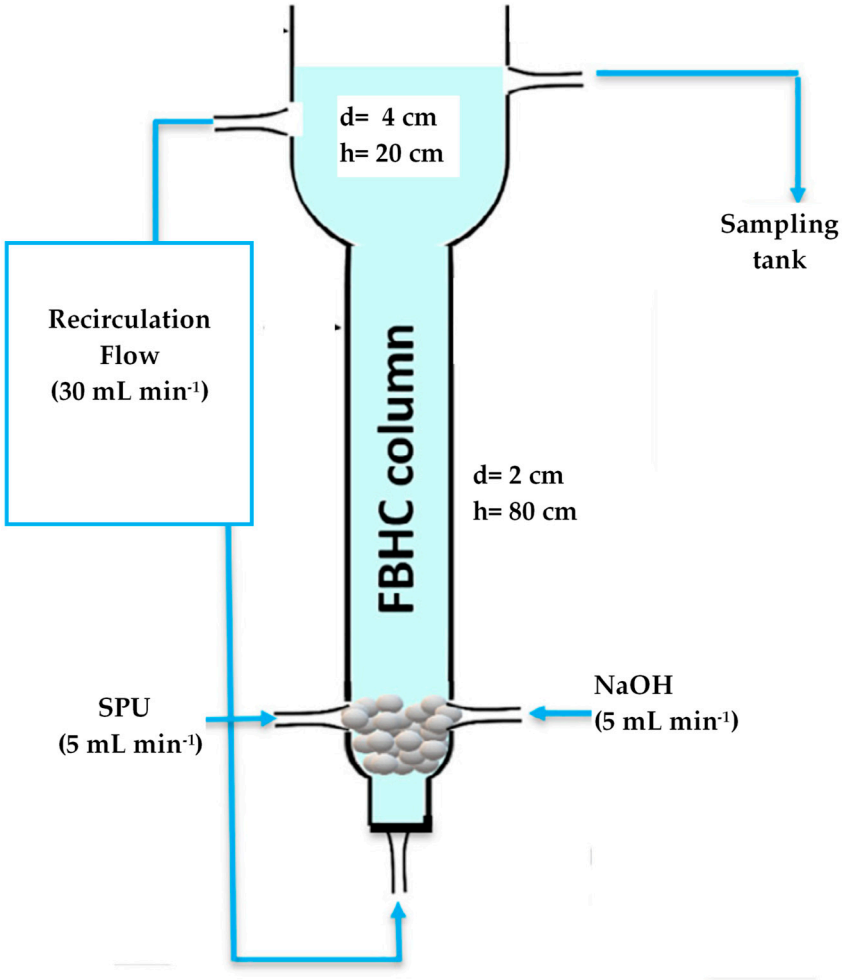

Figure 5. The FBHC column used in the study by Le et al. [30]. Reprinted/adapted with permission from Elsevier.

In another study [67], a pilot-scale FBR with a seeding application (Figure 6) was operated to produce MPP pellets from the SPU. During the stable operation of the FBR, a small amount of fine crystals that were formed by the attrition and breakage of MPP pellets flew out from the top section of the reactor. For instance, a superficial velocity of 450 $cm \cdot m^{-1}$ resulted in the formation of fines by breakage of the pellets due to intense

turbulence inside the FBR. Therefore, 350 cm·m^{-1} was reported as an optimum superficial velocity for their operational conditions to ensure the suspension of all pellets and to promote product growth. Primary nucleation was also observed during FBR operation at supersaturation ratios higher than 3. Hence, a supersaturation ratio of 3 was recommended as an upper limit to prevent the formation of fines by uncontrolled nucleation.

The draft tube and baffle reactor (DTBR) is another type of reactor used in K-struvite crystallization for simultaneous K and P recoveries from SPU and SSHU. Xu et al. designed a DTBR as depicted in Figure 7 [19,29,75]. As will be discussed in detail in Section 4.1, the effects of the operational parameters; i.e., mixing speed, hydraulic retention time (HRT), and crystal retention time (CRT) on the process performance were explored [29]. Their data proved that both the mixing speed and HRT had a significant effect on the crystallization and crystal-settling character. The frequency of slurry discharge in terms of CRT is another important operational parameter; the DTBR should be operated at a certain CRT (11 h for their experimental conditions) to ensure fluidity in the reactor. An increase in the interface of the reaction zone was also observed for an excess amount of slurry.

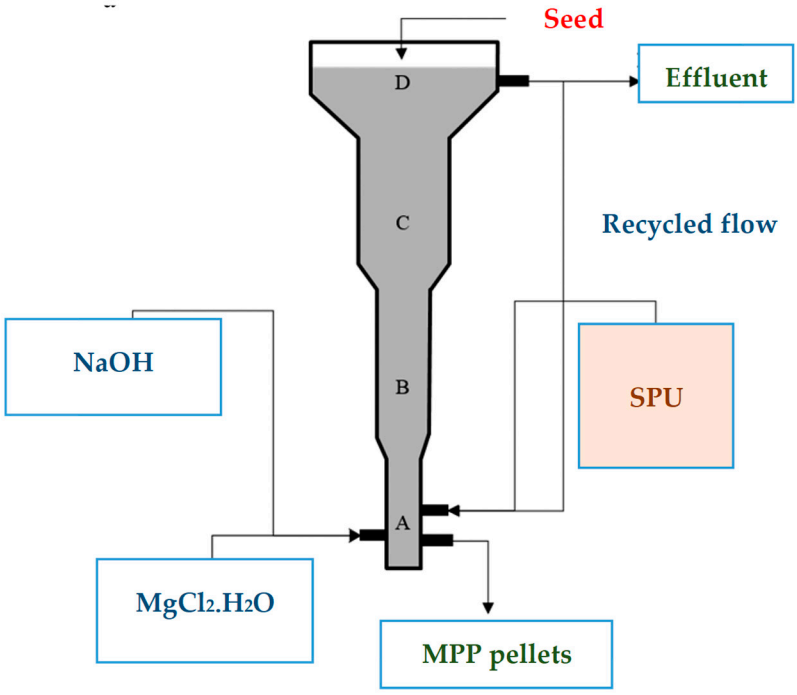

Figure 6. The pilot-scale FBR setup operated by Zhang et al. [67]. Reprinted/adapted with permission from American Chemical Society.

A bubble column with draft tube reactor was the reactor type utilized for simultaneous K and P recovery in some studies [15,50]. The shear stress and adhesion of particles to the surfaces in a BCRDT are lower than those produced in mechanical stirring because fluid circulation is provided by means of the pressure difference created by the air fed into the draft tube. Although the capability of such a reactor in the recovery of nutrients from livestock water drainage [50] and SPS [15] has been reported, no information on its operational conditions or associated problems were available in the relevant literature.

Even though findings proved the applicability of the above-mentioned reactors in nutrient-recovery applications using K-struvite precipitation at the lab scale, some problems were evident during their operations. Scaling on the reactor walls and downstream conduits due to poor mixing or suspension conditions and the formation of fine crystals due to uncontrolled primary nucleation or breakage of pellets were among the frequent operational problems that resulted in an unsatisfactory process performance. Therefore,

further studies are required to overcome these operational problems. Additionally, we should note that the performance of the above-mentioned reactors has not been tested yet for K-struvite applications at a large scale. On the other hand, continuous operation is applicable to plants that treat large amounts of waste streams, as in the case of anaerobic treatment digestate and central treatment plants. A continuous mode of operation also requires a relatively stable influent quality. Batch systems are much more versatile and easier to operate. Batch operation provides flexibility to cope with operational problems as well as a varying influent quality. The reactor performance depends on wastewater quality, operation conditions, and scaling and similar operation problems. Therefore, the suitable reactor type should be determined for each application while considering all these variables.

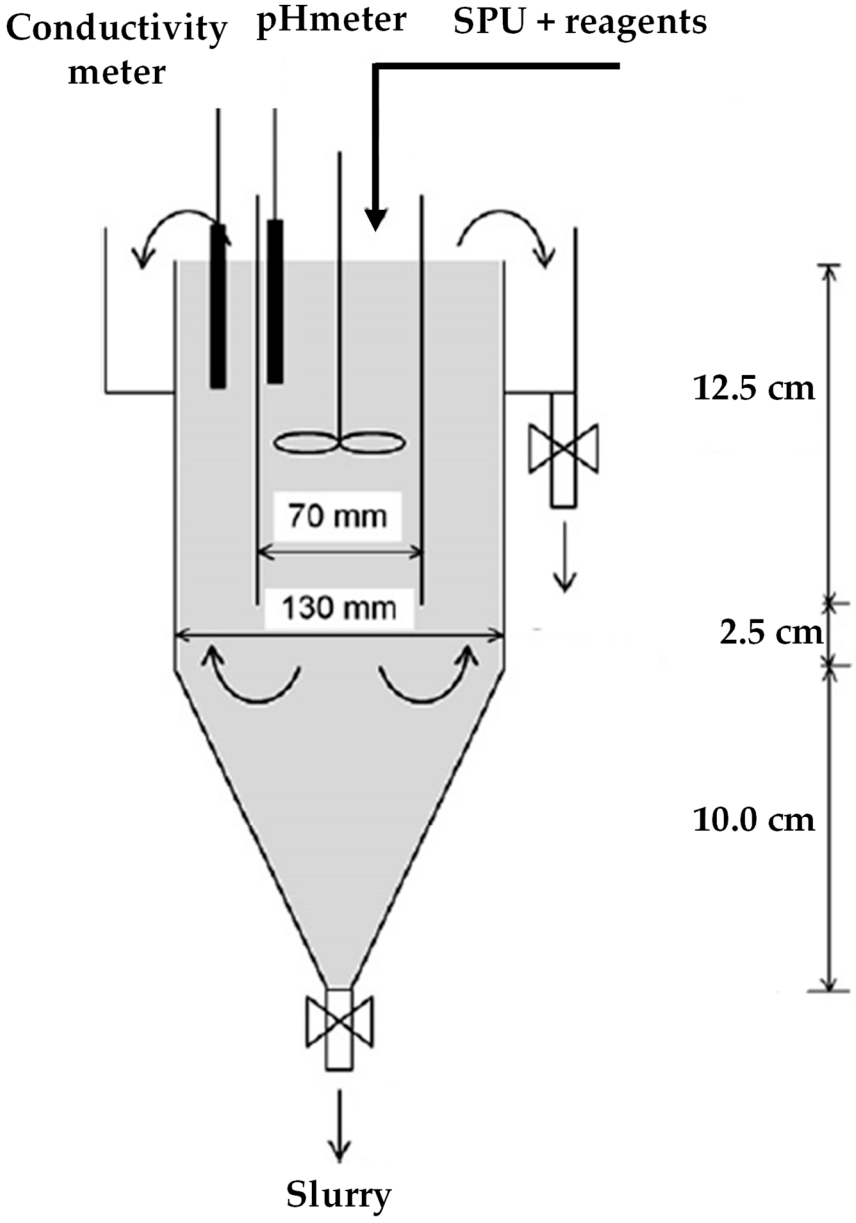

Figure 7. The DTBR used in the studies by Xu et al. [29]. Reprinted/adapted with permission from Elsevier.

4. Nutrient Recovery by K-Struvite Precipitation

4.1. Nutrient Recovery by K-Struvite Precipitation from Human Urine

In the last decade, K-struvite precipitation has been applied to either SPU or SSHU to recover potassium and phosphorous simultaneously. The SPU was simulated using the recipes that differed slightly in composition (Table 3). In these recipes, urea and ammonium chloride additions were generally omitted to eliminate ammonia interference and to induce K-struvite crystallization [14,19,29,30,67,75]. In some studies, precipitation applications were realized using specific crystallization reactors such as a lab-scale draft tube and baffle reactor, a CSTR, or an electrocoagulator with a magnesium anode, as elaborated in Section 3.4. Sometimes, external Mg and/or P sources were utilized to maximize the process performance. These studies that focused on simultaneous nutrient recovery from human urine by K-struvite can be summarized as follows.

Table 3. Recipes for synthetic human urine used in the studies.

Reagent	References			
	[14,19,29,30,75][a]	[67] [a]	[13] [b]	[32] [a]
$CaCl_2 \cdot 2H_2O$	4.4	0.7	0.09 [c]	0.5 [c]
$MgCl_2 \cdot 6H_2O$	3.2		0.04	1.5
NaCl	78.7	78.7	2.5	209
Na_2SO_4	16.2	16.2	0.98	16.5
Na_3-citrate$\cdot 2H_2O$	2.6			
Na_2-$(COO)_2$	0.15			0.25
KH_2PO_4	30.9	30.9	0.179 + 1.155 [d]	25
KCl	21.5	21	0.955	24
NH_4Cl	3.71	2.86	0.021	
$C_4H_7N_3O$ (ceratinine)	9.7			9.5

[a] mM; [b] g L^{-1}; [c] $CaCl_2$; [d] $Na_2HPO_4 \cdot 12H_2O$.

In a study by Xu et al. [14], the simultaneous recovery of K and P from the SPU through K-struvite precipitation was experimentally investigated. The results of bench-scale experiments indicated that both the solution pH and the molar ratio of Mg:K:P played a determining role in the process performance in the absence of ammonia. Increasing the solution pH improved K and P recovery efficiencies in the pH range of 7–11 at a molar ratio of 1.6:1:1.6, whereas K recovery efficiency decreased at pH 12. Although pH 11 was reported as an optimum value, their further experiments were performed at pH 10 to minimize the sodium addition. Similarly, the process performance was significantly enhanced with increasing molar ratios of Mg:K and P:K at a fixed molar ratio of Mg:P (1:1). On the other hand, the presence of ammonia (40–500 mg·L^{-1}) in the reaction solution at a molar ratio of 2:1:2 had a negative effect on the K recovery efficiency due to the co-precipitation of MAP and MPP. The ammonia precipitation efficiency decreased from 97 to 73% when the initial ammonia concentration in the SPU was increased from 40 to 500 mgN·L^{-1}.

In another study by Xu et al. [29], K-struvite crystallization was realized in a lab-scale draft tube and baffle reactor (DTBR). The SPU without ammonia and the ammonia-stripped SSHU (both diluted 5 times) were used in their study. The effects of mixing speed (50–300 rpm at HRT of 10 h) and hydraulic retention time (HRT; 2.5–12.5 h at 150 rpm) on the process performance were determined using the diluted SPU. In the range of 100-300 rpm, the mixing speed had no significant effect on the K (78–80%) and P (51–54%) recovery efficiencies. On the other hand, an increase in HRT from 2.5 to 12.5 h caused a decrease in the P recovery efficiency from 68 to 46% while improving the K recovery efficiency from 72 to 80%. A mixing speed higher than 250 rpm and HRTs of 2.5 and 5 h resulted in poor crystal settleability. Based on the results obtained for the SPU, they suggested that the DTBR should be operated at a mixing speed ≤ 200 rpm and an HRT ≥ 7.5 h to achieve high K and P recovery efficiencies and to produce crystals with good settling characteristics. When ammonia-stripped/diluted SSHU was fed into the DTBR, a mixing speed of 150 rpm

and an HRT of 10 h provided 76% K and 68% P recovery efficiencies. The DTBR was also operated to optimize the recovery of N, P, and K from the thrice-diluted SSHU in combinations of air stripping and precipitation [75]. In the first scenario, the effluent obtained from the struvite precipitation was fed into the air-stripping column. While 95% ammonia and 83% P recovery were obtained by this sequence, no K-struvite precipitation took place. The complete recovery of N, P, and K that was targeted by the other scenarios began with ammonia stripping, which was aerated at an airflow rate of 1 (Scenario II) or 1.5 $m^3 \cdot h^{-1}$ (Scenarios III and IV). Increasing the airflow rate from 1 to 1.5 $m^3 \cdot h^{-1}$ in the stripping column induced ammonia removal and the initial ammonia concentration (2393 mg N L^{-1}) was reduced from 169 ± 26 mg$N \cdot L^{-1}$ to 26 ± 18 mg $N \cdot L^{-1}$. Then, the air-stripped effluents were fed into the DTBR, which was operated at a mixing speed of 300 rpm and at molar ratios (Mg:K:P) of 3:1:3 (II and III) and 3.5:1:3 (V). An almost complete ammonia removal (99.9%) was achieved at the end of all three scenarios. When the magnesium dose was increased to 3.5 mole (Mg:K:P of 3.5:1:3), both P and K recoveries were enhanced (from 45 to 79 % and from 48 to 80%, respectively). The results of the scenarios commenced by air stripping indicated that: (i) K-struvite precipitation from the human urine did not take place unless the ammonia was previously removed; (ii) the precipitate consisted of a mixture of MAP, MPP, and MSP; and (iii) K recovery together with N and P proved to be an expensive option because the Mg and P requirements would increase due to the inevitable coprecipitation of MSP.

Zhang et al. [67] studied the simultaneous recovery of K and P from SPU simulated according to the recipe given in Table 3 in both a stirred crystallizer (CS) using a two-paddle agitator and a pilot-scale fluidized bed reactor (FBR). In their batch experiments, the parameters that affected the K-struvite crystal size were investigated by changing the initial pH from 8 to 11, the Mg:P molar ratio from 0.3 to 0.8, the mixing speed from 100 to 700 rpm, and the feeding volume of Mg from 10 to 30 mL in 1.5 L of SPU. Based on their data, it was concluded that: (i) increasing the initial pHs and Mg:P molar ratios led to the formation of small crystal sizes; (ii) an increase in the agitation speed from 100 to 700 rpm promoted the formation of large crystal sizes (72–114%); (iii) as the feed volume of Mg solution was increased, the average crystal size was reduced from 18 to 14 μm at 100 rpm; and (iv) at low pH (8) $Ca_3(PO_4)_2 \cdot 22H_2O$ and high pH values (>10.5), MSP coprecipitated together with MPP at a high molar ratio of Mg:P (0.7–0.8).

In the continuous experiments by Zhang et al. [88], the FBR was operated in different operation conditions to maximize the nutrient recovery and to produce large-sized MPP. SPU diluted two times was used in their experimental study. The operational parameters were tested at pHs of 9.5–11.0 and molar ratios of Mg:P of 0.6–1.6 at a fixed superficial velocity of 180 $cm \cdot min^{-1}$ and superficial velocities of 20–450 $cm \cdot min^{-1}$ at pH 10.5 and Mg:P of 1:1. At every tested Mg:P molar ratio, an increase in pH up to 10.5 improved both the K and P recovery efficiencies; beyond this, further enhancement by pH was not obtained. Excess doses of Mg (1.3 and 1.6) enhanced the K recovery efficiency, whereas almost equal P recovery efficiencies were obtained at stoichiometric and excess doses of Mg, particularly at pH 11.0. The crystal size was positively affected by increasing the superficial velocity from 20 to 450 $cm \cdot min^{-1}$, achieving a maximum average pellet size of 0.87 mm. This enhancement in the crystal size was attributed to an acceleration of the mass transfer ratio and the agglomeration of small crystals that were bound together by increasing the turbulence. Considering their pilot-scale results, a pH of 10.5, a stoichiometric dose of Mg/P (1 mole/1 mole), a superficial velocity of 350 $cm \cdot min^{-1}$, and a supersaturation ratio of 3.0 were determined to be the optimized operation conditions for the FBR. At these optimum values, 20–35% K and 80–90% P recovery efficiencies were attained and pellets (high purity of 86 ± 2%) with a maximum size of 4 mm were produced. Based on their data, a kinetic model for the MPP pellet growth rate (G) was proposed as follows:

$$G = 5.046 \times 10^{-9} \times SV^{0.88} \times S^{1.96} \quad (14)$$

where SV is the superficial velocity ($m \cdot s^{-1}$) and S is the supersaturation ratio.

In another study, simultaneous nutrient recovery from the SPU was realized using a FBHC reactor [30]. The up-flow velocity (U=10-50 $m \cdot h^{-1}$ at pH 10 ± 0.2 and Mg:P molar ratio of 1.5), pH (7–12 at Mg:P molar ratio=1.5 and U = 30 $m \cdot h^{-1}$), and Mg:K molar ratio (0–2.0 at pH 10 ± 0.2 and U= 30 $m \cdot h^{-1}$) were optimized for the initial concentrations of 1830 $mgK \cdot L^{-1}$ and 850 $mgP \cdot L^{-1}$. The optimized operational conditions were determined to be a solution pH of 10 ± 0.2, a Mg:K molar ratio of 1.25, and an up-flow velocity of 30$m \cdot h^{-1}$ for the FBHC reactor developed. Recovery efficiencies of 98.4% for P and 70.5% for K were achieved using an FBHC operation performed under the optimized operational conditions. After 400 h of FBHC operation, K-struvite granules with an average size of 0.85 mm and a purity of 95 ± 3% were produced. A mechanism for K-struvite granulation in the FBHC reactor that was proposed by Le et al. [30] is shown in Figure 8.

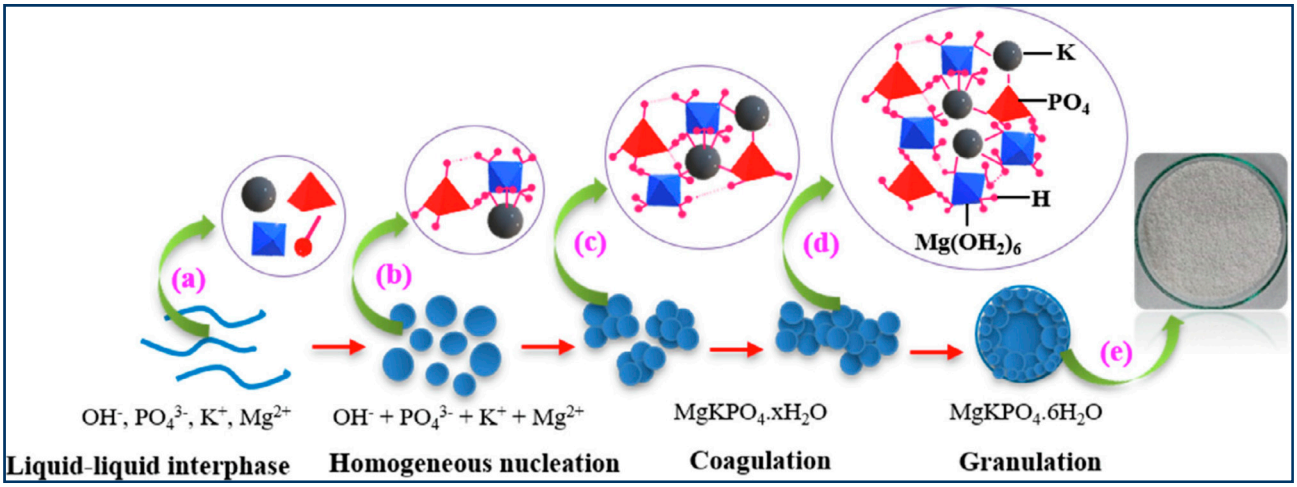

Figure 8. Mechanism proposed for homogeneous granulation of K-struvite: (**a**) liquid-liquid interphase, (**b**) homogeneous nucleation, (**c**) coagulation, (**d**) granulation, (**e**) produced precipitate; by Le et al. [30]. Reprinted/adapted with permission from Elsevier.

Shan et al. [13] electrochemically produced Mg to utilize in the simultaneous crystallization of K-struvite from SPU. The electrocoagulator was equipped with a magnesium plate anode (7 × 7 × 0.2 cm) and a universal steel wire mesh (70-mesh) cathode (7 × 7 × 0.2 cm). The effect of the current density (1.0–5.0 $mA \cdot cm^{-2}$) on the process performance was determined. At a K:P molar ratio of 1:0.25 and at a solution pH of 9.4, a white precipitate was formed at current densities of 1.0 and 1.5 $mA \cdot cm^{-2}$ after an electrolysis time of 60 min. K and P recoveries were reduced by increasing the current density; 74.6% P and 15.0% K recoveries were obtained at 1.5 $mA \cdot cm^{-2}$, whereas after 150 min, electrolysis P and K recoveries decreased by 61.6% and 12.2% at 2.0 $mA \cdot cm^{-2}$, respectively. Since the reduction in the process efficiency with an increasing current density was explained by a low reaction pH and a lack of P (P:K = 0.25), an external P source was dosed to increase the P:K ratio to 0.6. The white precipitate was formed by the P dosage at shorter electrolysis times of 30 and 10 min for 1.0 and 5 $mA \cdot cm^{-2}$, respectively. At the optimum current density of 3.5 $mA \cdot cm^{-2}$ and at a P:K molar ratio of 0.6, 88.5% P and 35.4% K were recovered in the form of rod-shaped K-struvite. Increasing the current densities induced the formation of the rod-like precipitate with more amorphous impurities (MSP and $Ca_3(PO_4)_2$) on the surface.

Huang et al. [32] conducted a comparative study to alleviate sodium's effect on the process performance and to produce K-struvite with a high purity from SPU. Within this context, $MgCl_2 \cdot 6H_2O$, an Mg sacrificial electrode, and $Mg(OH)_2$ were utilized as external Mg sources. Their experimental data indicated that: (i) elevating the solution pH from 8.5 to 12.0 augmented the MSP formation; and (ii) the maximum sodium content in the precipitate and P recovery efficiency were determined at pH 12, and above this pH, the formation of MSP declined due to $Mg_3(PO_4)_2$ precipitation. Similarly, an increase in the Na^+

concentration (in the range of 100–700 mM) accelerated the formation of MSP, which resulted in an enhancement in the P recovery efficiency (96%) and an increase in the sodium content in the precipitate (67 $mg \cdot g^{-1}$). When $MgCl_2$ was utilized as an external magnesium source, the reaction time had only a small effect on the process performance because the K and P recoveries reached their maximum values of 69.7% and 97.6%, respectively, within 5 min and remained practically unchanged when extending the reaction times. In the case of intermittent $MgCl_2$ dosing (P:K molar ratio of 1.6:1 and pH 11.5), K recovery efficiency was enhanced from 72 to 78% when the number of the times of intermittent dosage was increased from one to nine and the Na^+ content in the precipitate recovered was simultaneously increased. During the electrochemical (EC) application, the solution pH rose rapidly within the first 150 min and then gradually plateaued at all current densities tested. The time-dependent changes in both the K and P recovery efficiencies followed a similar pattern: the recovery efficiencies progressively improved by increasing the current density and extending the reaction time. At the end of 300 min of EC operation, the K and P recovery efficiencies reached those with the use of $MgCl_2$. An increase in the current density had an adverse effect on the K content in the recovered precipitate due to the coprecipitation of MSP and $Mg(OH)_2$. Another disadvantage of EC was reported as the formation of $Mg(OH)_2$ film covering the anode surface. The usage of $Mg(OH)_2$ as the magnesium source yielded the lowest K and P recovery efficiencies due to its dissolution problem. Around 50% recovery efficiencies were obtained when the Mg:K molar ratio was varied in the range of 1.5–5.5. In view of their data, $MgCl_2$ proved to be the most suitable magnesium source for the K-struvite crystallization from the SPU, followed by the Mg sacrificial electrode and $Mg(OH)_2$.

In another comparative study by Huang et al. [71], K and P were simultaneously recovered from SSHU with K-precipitation performed using low-grade MgO (LG-MO) derived from the calcination of magnesite mineral as an external magnesium source. An ammonia-stripped SSHU (pH 10.3 ± 0.1, K^+ 49.8 ± 2.8 mM, PO_4^{3-} 23.4 ± 1.1 mM, Na^+ 298 ± 10.3 mM, NH_4^+ 1.1 ± 0.03 mM, Mg^{2+} 0.06 ± 0.03 mM, Ca^{2+} 0.08 ± 0.01 mM) was used in their precipitation experiments. An LG-MgO addition was made in three different modes; namely, (i) alone (M1); (ii) together with H_3PO_4 (M2); and (iii) as a stabilizing agent (SA) preformed with H_3PO_4 (M3). In the M1 case, the addition of LG-MgO at an Mg:K:P molar ratio of 2:1:0.47 provided complete phosphate and only 25% K recovery efficiencies. In this case, the recovered precipitate was composed of a mixture of MPP (50%), MSP, and $Mg_3(PO_4)_2$. To enhance the K recovery efficiency, H_3PO_4 was dosed together with LG-MgO to reach different Mg:K:P molar ratios in the M2 case. At all tested molar ratios, the pH increased rapidly within the first 60 min and then remained practically constant around 10.7. An MgO:K:P molar ratio of 4:1:1.6 yielded the highest K recovery efficiency (70%) together with complete P recovery. Needle-like MPP crystals were coprecipitated with MSP and nonreacted MgO in this case. The SA used in the M3 case was mainly composed of $MgHPO_4 \cdot 3H_2O$ and MgO. An SA optimum dose of 8.2 $g \cdot L^{-1}$ corresponding to an MgO:K:P molar ratio of 1.5:1:1.5 provided the same K recovery efficiency (71%) as that of M2, but a lower P recovery efficiency (82%) than that of M2. Additionally, the competitive level of MPP and MSP was assessed by using batch experiments run at different pHs (10–12) and in a wide range of the Na:K ratio (5–30). The findings indicated that: (i) the effect of the solution pH on the competitive precipitation of MPP and MSP was negligible; (ii) the coprecipitation of MSP was promoted by elevating the Na concentration; and (iii) when the Na:K molar ratio exceeded 10, Na could compete with K for more P and Mg because the competitive ratio was over 1.

Gao et al. [23] performed continuous-flow experiments to simultaneously recover K and P from SPU and SSHU. After achieving the remaining ammonium concentration of 4–6 mM by air stripping at a gas–liquid ratio of 4800:1 at an initial pH of 11.5 in both the samples, K-struvite precipitation was accomplished at a K:Mg:P molar ratio of 1:1:1, a pH of 11 ± 0.1, and a flow rate of 4 $L \cdot h^{-1}$, corresponding to an HRT of 1h. For the SPU, 64 ± 2% K and 96 ± 1% P recovery efficiencies together with an MPP purity of 68.5 ± 2% were

attained by this application. Although an almost identical P recovery efficiency was obtained, the K recovery efficiency was reduced to 58.8 ± 2.4% in the case of the SSHU. A similar reduction but with a slightly higher impurity level was observed for the SSHU (60.4 ± 1.3%).

4.2. Other Sources

Many types of sewage and wastewater are characterized by high nutrient concentrations that are potentially recoverable through precipitation processes. Several works aimed at the recovery of nutrients in the form of struvite were available in the literature, while few papers focused their attention on the precipitation of K-struvite. Despite this, some researchers investigated K-struvite production from cattle manure [55,56], swine wastewater [59], poultry manure [89,90], agro-industrial waste or residual crops [26,31,91], and industrial wastewater [27] (Table S1).

4.2.1. Livestock Wastewater

The availability of nutrients in livestock wastewaters depends on their chemico-physical characteristics and storage and processing methods [92]. These wastewaters are commonly characterized by a low magnesium content compared to that of nutrients. Therefore, it is generally necessary to feed an external magnesium source to allow the nucleation and growth of struvite-type crystals [72,93,94].

Clearly, the complexity and heterogeneity of livestock effluents make the precipitation process rather difficult. The presence of many dissolved ions can hinder K-struvite formation. In particular, the simultaneous precipitation of MPP and MAP was often detected at a low ammonia nitrogen content [89,95].

In this regard, Huang et al. [59] carried out a study on K-struvite recovery using synthetic swine wastewater and plant ash as an alkalinizing reagent. The study identified the precipitation interference that occurred between MAP and K-struvite in wastewater with the simultaneous presence of N and K in a pH range between 8 and 10.5 and a K:N molar ratio of 1:1. The results showed that the presence of K in the solution limited the MAP formation and that there was a reduction in the MAP purity from 84% to 63% with the increase in pH [59]. At the same time, the authors showed an increase in K-struvite formation at a pH of 10. The authors also evaluated the effects of an increase in the K:TAN (corresponding to NH_3-N) ratio from 1 to 6 at pH 9.5. The results showed that as the K:TAN ratio was increased, the MAP recovery decreased while K-struvite recovery increased [59]. The precipitation of the two compounds was equivalent at a K:TAN of 6 with a purity of 43% for both crystal types and an overall P removal of 80%. These results confirmed that the formation of K-struvite can compete with MAP only when an excess of potassium is available in the liquor [59].

Zeng and Li [95] studied the recovery of nutrients (phosphate, ammonium, and potassium) from digested cattle manure after a centrifugation process. The authors assessed the precipitation process with and without a phosphate addition. They also studied the influence of the Mg/P and P/N ratios, pH (between 7 and 10), temperature (between 5 and 50 °C), and reaction time. The authors found that the removal efficiency of potassium was significantly lower than that of ammonium [95]. The molar percentage of precipitated K was always less than 10% of the total NH_4^+ removed. At pHs of 9 and 10 and without pretreatment of the livestock manure digestate, the formation of MAP exceeded that of K-struvite [95] (Table S1).

Tarragò et al. [56] investigated MPP recovery from the liquid fraction of manure. The precipitation process was carried out after solid/liquid separation and ammonia nitrogen removal using partial nitrification followed by an Anammox process. The authors firstly assessed the operating conditions to promote the K-struvite formation; a pH of 10 was identified as optimal at a temperature of 38°C. The established operational conditions were applied for the treatment of mixtures with manure percentages of 0–10–50–100% to assess the feasibility of K-struvite recovery [56]. At a lower manure content of 0–10%,

coprecipitation of K-struvite, magnesium phosphate, and magnesium hydroxide occurred. Indeed, the precipitate was characterized by different molar amounts of phosphate and potassium, indicating that not all the phosphorus was recovered in the form of K-struvite [56]. On the contrary, all the phosphate precipitated as K-struvite with manure contents of 50% and 100%. Despite this, the phosphate recovered from the mixtures with manure percentages of 50–100% (1.09 ± 0.12 mmolsPO_4^{3-} per liter treated) was half that recovered from the 0–10% manure mixtures (2.24 ± 0.06 mmols PO_4^{3-} per liter treated). The authors attributed the decrease in the phosphorus recovery to the higher content of solids in the mixtures [56]. They also postulated that the greater ionic strength of the matrices could have affected the K-struvite formation. Typical needle-like crystals with dimensions between 50 and 100 μm were found with a low content of solids (0–10% manure mixtures), whereas aggregates (with a star/asterisk form) of the needle-like crystals were observed when the content of solids was the highest (50–100% manure mixtures). Based on these observations, the authors argued that the presence of suspended particles favored both the nucleation phase and the crystal growth [56]. According to the authors, the suspended particles promoted the formation of linking bonds between crystals, enhancing their aggregation and causing a change in the overall morphology. The formation of large aggregates is clearly a positive aspect even if their separation from the sludge produced from the treatment of a real waste remains a challenging aspect.

Reach et al. [90] evaluated the recovery of nutrients in the form of struvite from poultry manure subjected to a thermochemical process. In this regard, the solid phase of the manure was incinerated and the resulting ashes were successively acidulated. Struvite was produced from the acidified ash extract after Mg and KOH additions at a pH of 8.5. The removal efficiency of P from treated poultry manure reached 90%. The recovered solids had high levels of macronutrients (P and K) and low levels of micronutrients and heavy metals [90]. Specifically, the precipitate was mainly composed of struvite and K-struvite with appreciable amounts of potassium sulphate and hydroxyapatite carbonate.

4.2.2. Agro-Industrial Waste

Similar to what we discussed in the previous paragraph, the production of K-struvite from agro-industrial wastes is a problematic process due to the high organic matter contents and a nitrogen concentration in the range 1–4 $g \cdot kg^{-1}$ [31,92]. Commonly, to avoid N interference phenomena, K-struvite precipitation is applied on pretreated agro-industrial waste. Some works focused on the recovery of K-struvite from waste after thermochemical treatments such as gasification and pyrolysis [31,91]. The outflows from the pyrolysis or gasification of agro-industrial biomass were characterized by a phosphate amount that could be much greater than that of nitrogen [96,97]. Indeed, during thermochemical reactions, ammonium nitrogen could be converted to gaseous ammonia and pass into the gas phase. The resulting liquid effluent brought about a low nitrogen and high phosphate content [31,97]. In this regard, Siciliano et al. [31] studied an integrated treatment process for the recovery of energy and K-struvite from agro-industrial wastes. Initially, the authors evaluated the biogas production yield from two different mixtures of agro-industrial wastes. In the second phase, the digestates were used for syngas production through supercritical water gasification (SCWG) at 450 °C and 250 bar. Finally, in the last step of the integrated treatment, the authors recovered the phosphorus in the form of K-struvite from the residual liquid fractions from the SCWG. The authors conducted K-struvite precipitation experiments by testing pH values between 9 and 12 and Mg/P values of 1, 1.2, and 1.4. The optimal operating conditions were identified as a pH of 10 and a Mg/P = 1, which allowed a phosphorous recovery efficiency of about 94% [31]. The precipitate showed the presence of crystals with a shape typical of that of pure magnesium potassium phosphate that were mainly composed of Mg, K, P, and O, with only trace amounts of Ca and Si. The average amount of the elements corresponded to a Mg/K/P equimolar ratio, confirming the formation of K-struvite [31].

In another study, K-struvite recovery from crop waste after thermochemical processes was experimentally investigated [91]. K-struvite was precipitated from pyrolyzed pumpkin (*Cucurbita pepo*) waste. In particular, the pumpkin waste was decomposed at high temperatures (800°C), then potassium was extracted from the residue using ultrapure water and then crystallized by adding $NaH_2PO_4 \cdot 2H_2O$ and $MgCl_2 \cdot 6H_2O$. The pH was set at 9.5–10 and K:Mg:P molar ratios of 1:1:1 and 1:2:2 were tested. The precipitation was more efficient when the magnesium/potassium ratio and phosphorus/potassium ratio were 2; it was estimated that about 80% of the potassium could be recovered as K-struvite crystals [91] (Table S1).

Another work focused on K-struvite recovery from agro-industrial waste by membrane separation technologies. Barros et al. [26] studied the influence of different electrolyte solutions (Na_2SO_4, $MgSO_4$, K_2SO_4, and NH_4NO_3) on electrodialysis (ED) performance for the desalination of vinasse and potassium recovery. The study was performed using a mixed configuration composed of one monovalent selective cationic membrane and non-monoselective heterogeneous anionic and cationic membranes. Optimal conditions were obtained with $MgSO_4$ and NH_4NO_3. Usage of NH_4NO_3 source mainly favored the formation of MAP due to the high quantities of NH_4^+ in the concentrate, while $MgSO_4$ was preferable for the precipitation of K-struvite [26]. In particular, using magnesium sulfate and ammonium nitrate, 4.4 and 3.9 kg of MPP and 0 and 7.3 kg of MAP per m^3 of treated waste, respectively, were produced [26].

4.2.3. Industrial Wastewater

Due to the high content of N, K, and phosphate, a precipitation process for recovery of nutrients as K-struvite represents a suitable technology for semiconductor wastewater. Warmadewanthi and Liu [27] investigated the effect of the $Mg:PO_4^{3-}$ molar ratio for NH_4^+ and PO_4^{3-} recovery as struvite. $MgCl_2 \cdot 6H_2O$ was used as an external source of Mg. The PO_4^{3-} removal was around 47.4% at pH 9 and a $Mg:PO_4^{3-}$ ratio of 1, which increased with an increasing molar ratio, reaching a value of 92.1% with a $Mg:PO_4^{3-}$ of 3. However, the authors determined an absence of K-struvite and only the presence of MAP in the precipitate [27].

Other industrial wastewaters such as produced water were also used for K-struvite recovery. Produced water represents wastewater generated as a byproduct during oil and natural gas extraction [98]. These effluents often contain large amounts of dissolved inorganic compounds such as potassium, phosphate, magnesium, calcium, and ammonia nitrogen [99]. Hu et al. [99] investigated in detail the calcium interference in the recovery of nutrients in the form of struvite compounds from produced water. In particular, the authors firstly conducted batch experiments on raw water with a Mg:P ratio of 1:1 to 1:7 in a pH range of 8–10 [99]. Due to the high initial calcium concentration (4779 ± 105 mg/L) in the crude produced water, low recovery rates of 0.3–6.1% for NH_4^+ and 1.3–5.4% for K^+ were found [99]. Subsequently, in order to eliminate the calcium interference, the wastewater was subjected to a pretreatment of CO_2 stripping and the addition of sodium carbonate. The precipitation process was evaluated using the pretreated water by changing the Mg:N:P molar ratio from 1:1:1 to 1.8:1:1.8 and the pH from 8 and 10. The recovery of NH_4^+ and K^+ increased with an increase in the Mg:N:P molar ratio. A Mg:N:P value of 1.5:1:1.5 and a pH of 9.5 were found to be optimal for struvite precipitation, with recovery efficiencies for NH_4^+, K^+, and Mg^{2+} of 85.9%, 24.8%, and 96.8%, respectively [99].

Other studies investigated K-struvite recovery from landfill leachates [100,101]. Li et al. [100] used a nanofiltration (NF) membrane separation process coupled with a cation exchange membrane electrolysis (CEME) and a precipitation process to treat landfill leachate. Specifically, 99% of the potassium in the NF concentrate of landfill leachate was transported to the cathode after 8 h. Potassium was then recovered using precipitation of K-struvite. With this technique, a K recovery efficiency of approximately 53% was achieved (Table S1). Based on these results, the authors stated that the recovery of

potassium as MPP crystals from NF concentrates in the CEME system was a feasible process [100].

Wu et al. [101] investigated the recovery of nutrients from landfill leachate after a forward osmosis (FO) process. To study the interference of calcium in the K-struvite formation process, the authors performed tests on raw leachate and after a pretreatment for calcium removal. In particular, they used a pretreatment with Na_2CO_3 at Ca^{2+}/Na_2CO_3 molar ratios of 1:1, 1:1.2, 1:1.4, and 1:1.5. They found a low recovery of struvite in raw wastewater due to Ca^{2+} coprecipitation in the form of $Ca_3(PO_4)_2$. After calcium removal, the process resulted in a significant improvement of struvite recovery. In particular, 4.34 kg of struvite and 365.6 kg of water could be recovered from one cubic meter of treated leachate [101].

5. Challenges and Perspectives Ahead

5.1. Use of K-Struvite as a Fertilizer

The properties of struvite as a slow-release fertilizer have been widely recognized. In particular, its low solubility allows for a gradual nutrient release during the growing season. This avoids overloading the plants and soil with nutrients and prevents the risks of burning the roots of treated crops [102,103]. Moreover, the slow release of nutrients allows them to be effectively absorbed by vegetables, and therefore leachate and drainage are avoided [102,103]. This helps to reduce environmental issues such as contamination of groundwater and eutrophication of water bodies. Numerous studies in the literature investigated the fertilizing properties of struvite recovered from wastewater [104–107]. The fertilization yields of struvite were assessed in the cultivation of multiple plant species such as turfgrass, ornamental plants, and vegetables [104–109].

Regarding the fertilizer value of K-struvite, Liu et al. [109] investigated the release rate of nutrients from MPP. The experimental results proved that the solubilization of phosphate in deionized water was slower than that of potassium. The authors justified this observation with the transformation of K-struvite to $Mg_3(PO_4)_2$, which has a lower solubility than MPP. Due to this behavior, the P release could continue for an extended period [109].

Duck Ryu et al. [105] analyzed struvite produced from semiconductor-washing wastewater as a fertilizer in the cultivation of Chinese cabbage. The authors produced a precipitate composed of MAP but with a significant presence of K, which was attributed to MPP. The fertilizing effect of this precipitate was compared to that of some commercial fertilizers: complex inorganic, organic, and compost. The experimental results clearly proved that the growth of Chinese cabbage was better promoted when the struvite precipitate was used than when applying organic fertilizer and compost [105]. However, the highest growth rate was recognized with the complex fertilizer. The better fertilizing properties were attributed to the higher content of potassium of the complex fertilizer compared to that of struvite [105]. In this regard, the use of K-struvite appeared to be very favorable for fertilizing purposes. The authors also observed a significant amount of nutrients in the leaf tissues of cabbage grown with struvite such as nitrogen (N), phosphorous (P), potassium (K), calcium (Ca), and magnesium (Mg), as well as the absence of heavy metals such as cadmium (Cd), arsenic (As), lead (Pb), and nickel (Ni). This observation proved that the application in agronomic applications of a precipitate containing struvite-type compounds recovered from the treatment of semiconductor-washing wastewater does not pose a concern regarding the content of heavy metals [105].

Hidayat et al. [15] implemented a K-struvite precipitate on crop growth and compared it to a coffee-husk compost and unfertilized soil. Struvite produced from synthetic wastewater in a bubble column reactor was more effective in the growth of radish (*Raphanus sativus L.*) and komatsuna (*Japanese mustard spinach*) when compared to control and compost.

El Nakhel et al. [110] evaluated the use of processed urine fertilizers in the greenhouse soilless cultivation of lettuce (*Lactuca sativa* L.*).* Among eight different urine fertilizer products that were generated, MPP supported the growth of lettuce similar to that of a commercial mineral fertilizer. Moreover, K-struvite increased the accumulation of magnesium (+44.9%), which is an added value when the vegetables are supplemented in the daily diet.

The results of the few available works on the use of MPP as a fertilizer that were discussed above certainly supported the application of this compound in agronomic practices. However, the commercial use of struvite is allowed only in a few countries. Neither struvite nor K-struvite are included or recognized as a fertilizer in Europe. Despite this, the new EU fertilizer regulation ((EU) 2019/1009) [111] includes fertilizing compounds based on secondary raw materials. Among the various raw materials recoverable from the treatment of aqueous waste and wastewater, K-struvite could potentially become a component material in the new regulation ((EU) 2019/1009).

5.2. Economic Aspects of K-Struvite Precipitation

The environmental benefits of recovering struvite-type compounds from waste and wastewaters are numerous, including mitigating excessive nutrients enrichment of water bodies, saving natural resources, and reusing nutrients as fertilizers [39]. Nevertheless, economic sustainability is a fundamental aspect when assessing the real applicability of the struvite crystallization process in the field of waste and wastewater treatment.

In an economic analysis, the costs of construction, the expenses for the process operation and management, and the profits that could be obtained from the reuse and sale of recovered precipitate should be considered. The units commonly used for struvite precipitation processes are fairly simple reactors and separation units that require low construction expenses [1]. Therefore, in the economic analysis, the operational and management practices have the greatest impact. Specifically, the dosage of reagents and the energetic consumption are the main cost items. These costs are widely affected by the properties of the treated wastewater [1].

Compared to the recovery of MAP, the precipitation of K-struvite is potentially more sustainable. Indeed, MAP precipitation usually aims at the removal of NH_4^+ and a large amount of phosphorus reagents must be dosed to reach the required stoichiometric amount (due to a lack of P compared to N in real wastewater), which makes the process very expensive [31,44]. In the case of K recovery, the need for phosphate reactants and therefore the related costs are generally much lower. The other expenses for chemicals are due to the consumption of Mg sources and alkaline compounds. Clearly, the use of pure reagents increases the expense of treatment. For this reason, the identification of effective unconventional low-cost reactants is a main topic in the development of sustainable K-struvite precipitation processes. The application of air insufflation could allow a significant reduction in process costs. Indeed, the air flux ensures the mixing conditions and, in addition, allows regulation of the pH for K-struvite formation, saving the consumption of alkaline reagents [1].

While several papers carried out economic evaluations on MAP recovery from a variety of wastewaters, only few papers reported on economic estimations of the K-struvite precipitation process. The available analyses regarded the recovery of MPP from both synthetic and source-separated real urine. In particular, Huang et al. [32], estimated an overall cost per m^3 of synthetic urine of USD 3.61, USD 6.28, and USD 3.99 using $MgCl_2$ (with intermittent dosage), an Mg electrode, and $Mg(OH)_2$ as the magnesium source, respectively. The use of $MgCl_2$, in addition to having the lowest cost, resulted in the highest K removal (77%) and precipitate purity (65.3%). These findings were not consistent with those of some works that focused on MAP precipitation; according to these studies, compared to using $MgCl_2$, the utilization of $Mg(OH)_2$ can achieve a similar NH_4^+ removal with lower costs [32]. Moreover, it was also reported that the expense involved in using the Mg electrode was comparable to that of using $MgSO_4$ and $MgCl_2$ [71]. According to the

authors, the necessity of soluble magnesium salts in the crystallization of K-struvite to reach a higher ionic concentration was attributable to the different solubility product compared to that of MAP [17,32,68,71].

Huang et al. [71] also conducted an economic evaluation of source-separated real urine treatment using low-grade MgO (LG-MgO) with and without phosphorus sources. In particular, three different dosage modes were tested: LG-MgO alone (M1), LG-MgO together with H_3PO_4 (M2), and a preformed stabilizing agent (SA) that combined LG-MgO and H_3PO_4 (M3). In addition, the use of pure reagents only was evaluated. This last case, as expected, resulted in a higher cost compared to the three modes with low cost MgO. For the M1–M3 modes, higher costs were calculated for the second (USD 7.26·m^{-3}) and third modes (USD 8.52·m^{-3}), mainly due to the addition of phosphorus reagents. Costs related to the LG-MgO dosage were much lower. Moderate expenses for energy consumption were estimated. Furthermore, the economic value of the recovered product was included in the analysis while considering a sale price for the Chinese market for P products of USD 0.50·m^{-3}. In this way, the three tested processes resulted in a positive gain of USD 2.79, USD 5.42, and USD 2.90 per m^3 of treated urine, respectively. When using pure reagents instead, a negative economic outlay of USD 0.38·m^{-3} was calculated. Based on this analysis, it was evident that the K-struvite precipitation process is economically advantageous when unconventional reagents are utilized and if the recovered precipitate can be sold.

6. Conclusions

In this review, the theoretical background, main process parameters, type of reagents, and reactor configurations for K-struvite precipitation were presented. The recovery of MPP from various types of waste and wastewater was also analyzed and discussed. Finally, some considerations of the applicability of K-struvite as a fertilizer and of the economic sustainability of the process were reported. MPP generation is mainly affected by the pH, dosage, and type of reagents, as well as the presence of competitive dissolved elements. A fair variability of the values of the process parameters considered as optimal to obtain the best performance was found in the published papers. Regarding the process pH, the optimal values were reported to be between 9 and 11, and in most cases around 10. As for the Mg:K:P molar ratio, a stoichiometric value (1:1:1) is required to permit the formation of K-struvite crystals. However, overdosages of Mg^{2+} and PO_4^{3-} allow for an increase in the process performance. Depending on the type of external precipitating agents being used, overdoses of $Mg^{2+}$and PO_4^{3-} were applied up to 4- and 2-fold on a molar basis, respectively. In general, higher efficiencies were obtained using pure reagents.

As expected, ammonium was recognized as the main competitive ion for K-struvite formation due to the much lower solubility of MAP, which precipitates in the same pH range of MPP. Ammonium concentrations of around 30 mM were reported to prevent the precipitation of K-struvite. Calcium ions can also exhibit a strong inhibition power by reducing the availability PO_4^{3-} ions for K-struvite formation. The negative effect of calcium could be counteracted by the magnesium ions; for this purpose, a Mg/Ca ratio above 2 was considered necessary. Sodium is also a natural competitive ion because it promotes the precipitation of MSP crystals. The competition between sodium and potassium for precipitation is mainly regulated by the Na:K ratio, an increase in which reduces the MPP formation. On the contrary, for values lower than 2.1, no precipitation of MSP was observed.

The research activity paid great attention to the optimization of the reactor configurations for K-struvite precipitation and recovery. The STR and FBR were the most applied reactors and their effectiveness was widely proved. Despite this, efforts are constantly ongoing to further ameliorate these types of units and reduce some operational drawbacks. Moreover, other types of reactors such as DTBRs and BCRDTs were investigated.

Source-separated human urine is considered the most important target effluent for K-struvite production. Other aqueous wastes such as livestock effluents and agro-

industrial wastewater were also studied as possible matrices for MPP recovery. However, due to the complex characteristics of all these effluents and their high content of competitive ions, specific pretreatments were applied to remove the factors capable of hindering the formation and precipitation of MPP.

Knowledge of the fertilizing value of the K-struvite is still limited; nevertheless, the available data support its applicability in agronomic practices. The results of some economic analyses indicated that the recovery of nutrients through MPP precipitation became a profitable approach when low-grade reagents were used and the precipitate could be sold.

On the basis of the literature reports, it was clear that some aspects need further research to enhance the technology. In particular, the definition of sustainable pretreatments for a reduction in inhibition factors is a crucial topic to make the technology suitable for real effluents. Additional efforts should also be made to identify and test other types of low-cost unconventional sources for both magnesium and phosphorus that are exploitable as reagents in the precipitation process. Furthermore, with the aim to apply K-struvite as a slow-release fertilizer, technological improvements are required to produce crystals with a high purity and large dimensions so that they can be easily recovered and reused.

Supplementary Materials: The following are available online at www.mdpi.com/article/10.3390/su141811680/s1, Table S1: Results of MPP and MAP precipitation conducted on various wastes and using different reactors. References [14,15,17,23,26,27,29–32,44,50,56,59,62,67,71,75,89–91,94,95,99–101] are cited in the supplementary materials.

Author Contributions: Conceptualization, I.K. and A.S.; methodology, I.K., A.S., C.L. and O.T.; investigation, I.K., A.S., C.L. and O.T.; resources, I.K., A.S., C.L. and O.T.; data curation, I.K., A.S., C.L. and O.T.; writing—original draft preparation, I.K., A.S., C.L. and O.T.; writing—review and editing, I.K., A.S., C.L. and O.T.; visualization, I.K., A.S., C.L. and O.T. All authors have read and agreed to the published version of the manuscript.

Funding: This research received no external funding.

Institutional Review Board Statement: Not applicable.

Informed Consent Statement: Not applicable.

Data Availability Statement: Not applicable.

Acknowledgments: The authors from the University of Calabria would like to thank Regione Calabria (Italy) for a three-year research grant to C.L. (Bando DR. N. 1644/2019, Area Tematica S3 regionale "Ambiente e Rischi Naturali", SSD CHIM/07, Scheda Analitica A.9.2).

Conflicts of Interest: The authors declare no conflict of interest.

Abbreviations

MAP	Magnesium ammonium phosphate (struvite)
MPP	Magnesium potassium phosphate (K-struvite)
MSP	Magnesium sodium phosphate (S-struvite)
MP	Magnesium phosphate
SEM	Scanning electron microscopy
EDS	Energy-dispersive X-ray spectroscopy
EDTA	Ethylenediaminetetraacetic acid
SCWG	Supercritical water gasification
FT-IR	Fourier-transformed Infrared spectroscopy
SPU	Synthetically prepared urine
SPS	Synthetically prepared sample
SSHU	Source-separated human urine
SA	Stabilizing agent
LG-MO	Low-grade magnesium oxide
HAP	Hydroxyapatite

TCP	Tricalcium phosphate
OCP	Octacalcium phosphate
DCP	Dicalcium phosphate
DCPD	Dicalcium phosphate dehydrate
ACP	Amorphous calcium phosphate
STRs	Stirred-tank reactors
BSTR	Batch stirred-tank reactor
CSTR	Continuous stirred-tank reactor
FBRs	Fluidized bed reactors
FBHC	Fluidized bed homogeneous crystallization
DTBR	Draft tube and baffle reactor
BCRDT	Bubble column reactor with draft tube
CRT	Crystal retention time
HRT	Hydraulic retention time
Q	Hydraulic flowrate
V	Reactor volume
EC	Electrochemical
TAN	Total ammonia nitrogen
NF	Nanofiltration
CEME	Cation exchange membrane electrolysis
ED	Electrodialysis
FO	Forward osmosis
EU	European Union

References

1. Siciliano, A.; Limonti, C.; Curcio, G.M.; Molinari, R. Advances in Struvite Precipitation Technologies for Nutrients Removal and Recovery from Aqueous Waste and Wastewater. *Sustainability* **2020**, *12*, 7538. https://doi.org/10.3390/SU12187538.
2. Tünay, O.; Kabdaşlı, I.; Orhon, D.; Kolçak, S. Ammonia Removal by Magnesium Ammonium Phosphate Precipitation in Industrial Wastewaters. *Water Sci. Technol.* **1997**, *36*, 225–228. https://doi.org/10.1016/S0273-1223(97)00391-0.
3. Kabdaşlı, I.; Tünay, O. Nutrient Recovery by Struvite Precipitation, Ion Exchange and Adsorption from Source-Separated Human Urine—A Review. *Environ. Technol. Rev.* **2018**, *7*, 106–138. https://doi.org/10.1080/21622515.2018.1473504.
4. Tünay, O.; Kabdaşlı, I.; Mehmet, B. Nitrogen Removal and Recovery from Human Urine by Struvite Precipitation. *Int. J. Environ. Waste Manag.* **2009**, *3*, 382–392. https://doi.org/10.1504/IJEWM.2009.026353.
5. Kabdaşlı, I.; Tünay, O.; Işlek, Ç.; Erdinç, E.; Hüskalar, S.; Tatli, M.B. Nitrogen Recovery by Urea Hydrolysis and Struvite Precipitation from Anthropogenic Urine. *Water Sci. Technol.* **2006**, *53*, 305–312. https://doi.org/10.2166/WST.2006.433.
6. Kabdaşlı, I.; Tünay, O.; Özcan, P. Application of Struvite Precipitation Coupled with Biological Treatment to Slaughterhouse Wastewaters. *Environ. Technol.* **2009**, *30*, 1095–1101. https://doi.org/10.1080/09593330903136856.
7. Kabdaşlı, I.; Şafak, A.; Tünay, O. Bench-Scale Evaluation of Treatment Schemes Incorporating Struvite Precipitation for Young Landfill Leachate. *Waste Manag.* **2008**, *28*, 2386–2392. https://doi.org/10.1016/J.WASMAN.2007.10.020.
8. Kabdaşlı, I.; Atalay, Z.; Tünay, O. Effect of Solution Composition on Struvite Crystallization. *J. Chem. Technol. Biotechnol.* **2017**, *92*, 2921–2928. https://doi.org/10.1002/JCTB.5310.
9. Loewenthal, R.E.; Kornmuller, U.R.C.; van Heerden, E.P. Modelling Struvite Precipitation in Anaerobic Treatment Systems. *Water Sci. Technol.* **1994**, *30*, 107–116. https://doi.org/10.2166/WST.1994.0592.
10. Rahaman, M.S.; Mavinic, D.S.; Meikleham, A.; Ellis, N. Modeling Phosphorus Removal and Recovery from Anaerobic Digester Supernatant through Struvite Crystallization in a Fluidized Bed Reactor. *Water Res.* **2014**, *51*, 1–10. https://doi.org/10.1016/J.WATRES.2013.11.048.
11. González-Morales, C.; Fernández, B.; Molina, F.J.; Naranjo-Fernández, D.; Matamoros-Veloza, A.; Camargo-Valero, M.A. Influence of PH and Temperature on Struvite Purity and Recovery from Anaerobic Digestate. *Sustainability* **2021**, *13*, 10730. https://doi.org/10.3390/SU131910730.
12. Wang, L.; Gu, K.; Zhang, Y.; Sun, J.; Gu, Z.; Zhao, B.; Hu, C. Enhanced Struvite Generation and Separation by Magnesium Anode Electrolysis Coupled with Cathode Electrodeposition. *Sci. Total Environ.* **2022**, *804*, 150101. https://doi.org/10.1016/J.SCITOTENV.2021.150101.
13. Shan, J.; Liu, H.; Long, S.; Zhang, H.; Lichtfouse, E. Electrochemical Crystallization for Recovery of Phosphorus and Potassium from Urine as K-Struvite with a Sacrificial Magnesium Anode. *Environ. Chem. Lett.* **2022**, *20*, 27–33. https://doi.org/10.1007/S10311-021-01333-5.
14. Xu, K.; Wang, C.; Liu, H.; Qian, Y. Simultaneous Removal of Phosphorus and Potassium from Synthetic Urine through the Precipitation of Magnesium Potassium Phosphate Hexahydrate. *Chemosphere* **2011**, *84*, 207–212. https://doi.org/10.1016/J.CHEMOSPHERE.2011.04.057.

15. Hidayat, E.; Harada, H. Simultaneously Recovery of Phosphorus and Potassium Using Bubble Column Reactor as Struvite-K and Implementation on Crop Growth. In *Crystallizations and Applications*; Ben Smida, Y., Marzouki, R., Eds.; IntechOpen Limited: London, UK, 2021. https://doi.org/10.5772/INTECHOPEN.100103.
16. Kabdaşlı, I.; Kuşçuoğlu, S.; Tünay, O.; Siciliano, A. Assessment of K-Struvite Precipitation as a Means of Nutrient Recovery from Source Separated Human Urine. *Sustainability* **2022**, *14*, 1082. https://doi.org/10.3390/SU14031082.
17. Wilsenach, J.A.; Schuurbiers, C.A.H.; van Loosdrecht, M.C.M. Phosphate and Potassium Recovery from Source Separated Urine through Struvite Precipitation. *Water Res.* **2007**, *41*, 458–466. https://doi.org/10.1016/J.WATRES.2006.10.014.
18. Kuşcuoğlu, S. *Determination of K-Struvite Application Bases*; İstanbul Technical University: İstanbul, Turkey, 2008.
19. Xu, K.; Li, J.; Zheng, M.; Zhang, C.; Xie, T.; Wang, C. The Precipitation of Magnesium Potassium Phosphate Hexahydrate for P and K Recovery from Synthetic Urine. *Water Res.* **2015**, *80*, 71–79. https://doi.org/10.1016/J.WATRES.2015.05.026.
20. Yang, Y.; Liu, J.; Wang, B.; Liu, R.; Zhang, T. A Thermodynamic Modeling Approach for Solubility Product from Struvite-k. *Comput. Mater. Sci.* **2019**, *157*, 51–59. https://doi.org/10.1016/J.COMMATSCI.2018.10.037.
21. Bennett, A.M.; Lobanov, S.; Koch, F.A.; Mavinic, D.S. Improving Potassium Recovery with New Solubility Product Values for K-Struvite. *J. Environ. Eng. Sci.* **2017**, *12*, 93–103. https://doi.org/10.1680/JENES.17.00019.
22. Lothenbach, B.; Xu, B.; Winnefeld, F. Thermodynamic Data for Magnesium (Potassium) Phosphates. *Appl. Geochem.* **2019**, *111*, 104450. https://doi.org/10.1016/J.APGEOCHEM.2019.104450.
23. Gao, Y.; Liang, B.; Chen, H.; Yin, P. An Experimental Study on the Recovery of Potassium (K) and Phosphorous (P) from Synthetic Urine by Crystallization of Magnesium Potassium Phosphate. *Chem. Eng. J.* **2018**, *337*, 19–29. https://doi.org/10.1016/J.CEJ.2017.12.077.
24. Lee, S.-H.; Kumar, R.; Jeon, B.-H. Struvite Precipitation under Changing Ionic Conditions in Synthetic Wastewater: Experiment and Modeling. *J. Colloid Interface Sci.* **2016**, *474*, 93–102. https://doi.org/10.1016/J.JCIS.2016.04.013.
25. Zengin, G.; Ölmez, T.; Doğruel, S.; Kabdaşlı, I.; Tünay, O. Assessment of source-based nitrogen removal alternatives in leather tanning industry wastewater. *Water Sci. Technol.* **2002**, *45*, 205–215. https://doi.org/10.2166/wst.2002.0428.
26. Barros, L.B.M.; Brasil, Y.L.; Silva, A.F.R.; Andrade, L.H.; Amaral, M.C.S. Potassium Recovery from Vinasse by Integrated Electrodialysis—Precipitation Process: Effect of the Electrolyte Solutions. *J. Environ. Chem. Eng.* **2020**, *8*, 104238. https://doi.org/10.1016/J.JECE.2020.104238.
27. Warmadewanthi; Liu, J.C. Recovery of Phosphate and Ammonium as Struvite from Semiconductor Wastewater. *Sep. Purif. Technol.* **2009**, *64*, 368–373. https://doi.org/10.1016/J.SEPPUR.2008.10.040.
28. Shashvatt, U.; Benoit, J.; Aris, H.; Blaney, L. CO_2-Assisted Phosphorus Extraction from Poultry Litter and Selective Recovery of Struvite and Potassium Struvite. *Water Res.* **2018**, *143*, 19–27. https://doi.org/10.1016/J.WATRES.2018.06.035.
29. Xu, K.; Wang, C.; Wang, X.; Qian, Y. Laboratory Experiments on Simultaneous Removal of K and P from Synthetic and Real Urine for Nutrient Recycle by Crystallization of Magnesium–Potassium–Phosphate–Hexahydrate in a Draft Tube and Baffle Reactor. *Chemosphere* **2012**, *88*, 219–223. https://doi.org/10.1016/J.CHEMOSPHERE.2012.02.061.
30. Le, V.-G.; Vu, C.-T.; Shih, Y.-J.; Bui, X.-T.; Liao, C.-H.; Huang, Y.-H. Phosphorus and Potassium Recovery from Human Urine Using a Fluidized Bed Homogeneous Crystallization (FBHC) Process. *Chem. Eng. J.* **2020**, *384*, 123282. https://doi.org/10.1016/J.CEJ.2019.123282.
31. Siciliano, A.; Limonti, C.; Mehariya, S.; Molino, A.; Calabrò, V. Biofuel Production and Phosphorus Recovery through an Integrated Treatment of Agro-Industrial Waste. *Sustainability* **2019**, *11*, 52. https://doi.org/10.3390/SU11010052.
32. Huang, H.; Zhang, D.; Wang, W.; Li, B.; Zhao, N.; Li, J.; Dai, J. Alleviating Na^+ Effect on Phosphate and Potassium Recovery from Synthetic Urine by K-Struvite Crystallization Using Different Magnesium Sources. *Sci. Total Environ.* **2019**, *655*, 211–219. https://doi.org/10.1016/J.SCITOTENV.2018.11.259.
33. Banks, E.; Chianelli, R.; Korenstein, R. Crystal Chemistry of Struvite Analogs of the Type $MgMPO_4{\cdot}6H_2O$ ($M^+ = K^+$, Rb^+, Cs+, Ti^+, $NH4^+$). *Inorg. Chem.* **1975**, *14*, 1634–1639.
34. Mathew, M.; Schroeder, L.W. Crystal Structure of a Struvite Analogue, $MgKPO_4.6H_2O$. *Acta Crystallogr. Sect. B Struct. Crystallogr. Cryst. Chem.***1979**, *35*, 11–13. https://doi.org/10.1107/S0567740879002429.
35. Mathew, M.; Kingsbury, P.; Takagi, S.; Brown, W.E. A New Struvite-Type Compound, Magnesium Sodium Phosphate Heptahydrate. *Acta Crystallogr. Sect. B Struct. Crystallogr. Cryst. Chem.* **1982**, *38*, 40–44. https://doi.org/10.1107/S0567740882002003.
36. Graeser, S.; Postl, W.; Bojar, H.-P.B.; Armbruster, T.; Raber, T.; Ettinger, K.; Walter, F. Struvite-(K), $KMgPO_46H_2O$, the Potassium Equivalent of Struvite a New Mineral. *Eur. J. Mineral.* **2008**, *20*, 629–633. https://doi.org/10.1127/0935-1221/2008/0020-1810.
37. Ohlinger, K.N.; Young, T.M.; Schroeder, E.D. Predicting Struvite Formation in Digestion. *Water Res.* **1998**, *32*, 3607–3614. https://doi.org/10.1016/S0043-1354(98)00123-7.
38. Chauhan, C.K.; Vyas, P.M.; Joshi, M.J. Growth and characterization of Struvite-K crystals. *Cryst. Res. Technol.* **2011**, *46*, 187–194. https://doi.org/ 10.1002/crat.201000587.
39. Shih, K.; Yan, H. The Crystallization of Struvite and Its Analog (K-Struvite) From Waste Streams for Nutrient Recycling. *Environ. Mater. Waste: Resour. Recovery Pollut. Prev.* **2016**, 665–686. https://doi.org/10.1016/B978-0-12-803837-6.00026-3.
40. Ronteltap, M.; Maurer, M.; Hausherr, R.; Gujer, W. Struvite Precipitation from Urine—Influencing Factors on Particle Size. *Water Res.* **2010**, *44*, 2038–2046. https://doi.org/10.1016/J.WATRES.2009.12.015.
41. Frost, R.L.; Weier, M.L.; Martens, W.N.; Henry, D.A.; Mills, S.J. Raman Spectroscopy of Newberyite, Hannayite and Struvite. *Spectrochim. Acta Part A Mol. Biomol. Spectrosc.* **2005**, *62*, 181–188.

42. Zhang, S.; Shi, H.-S.; Huang, S.-W.; Zhang, P. Dehydration Characteristics of Struvite-K Pertaining to Magnesium Potassium Phosphate Cement System in Non-Isothermal Condition. *J. Therm. Anal. Calorim.* **2013**, *111*, 35–40. https://doi.org/10.1007/S10973-011-2170-9.
43. Gardner, L.J.; Walling, S.A.; Lawson, S.M.; Sun, S.; Bernal, S.A.; Corkhill, C.L.; Provis, J.L.; Apperley, D.C.; Iuga, D.; Hanna, J. v.; et al. Characterization of and Structural Insight into Struvite-K, $MgKPO_4 \cdot 6H_2O$, an Analogue of Struvite. *Inorg. Chem.* **2021**, *60*, 195–205. https://doi.org/10.1021/ACS.INORGCHEM.0C02802/ASSET/IMAGES/LARGE/IC0C02802_0008.JPEG.
44. Siciliano, A.; Stillitano, M.A.; Limonti, C.; Marchio, F. Ammonium Removal from Landfill Leachate by Means of Multiple Recycling of Struvite Residues Obtained through Acid Decomposition. *Appl. Sci.* **2016**, *6*, 375. https://doi.org/10.3390/APP6110375.
45. Lelet, M.I.; Yakun'kova, M.L.; Mikhailov, D.A.; Lelet, J.N. Experimental Calorimetric Study of Thermodynamic Properties of Two Magnesium Phosphates, $MgHPO_4 \cdot 3H_2O$ and $MgKPO_4 \cdot 6H_2O$. *J. Chem. Eng. Data* **2021**, *66*, 2723–2732. https://doi.org/10.1021/ACS.JCED.1C00067/ASSET/IMAGES/MEDIUM/JE1C00067_M028.GIF.
46. Luff, B.B.; Reed, R.B. Thermodynamic Properties of Magnesium Potassium Orthophosphate Hexahydrate. *J. Chem. Eng. Data* **1980**, *25*, 310–312. https://doi.org/10.1021/JE60087A028/ASSET/JE60087A028.FP.PNG_V03.
47. Snoeyink, V.L.; Jenkins, D. *Water Chemistry*; Wiley: New York, NY, USA, 1980; ISBN 9780471051961.
48. le Corre, K.S.; Valsami-Jones, E.; Hobbs, P.; Parsons, S.A. Phosphorus Recovery from Wastewater by Struvite Crystallization: A Review. *Crit. Rev. Environ. Sci. Technol.* **2009**, *39*, 433–477. https://doi.org/10.1080/10643380701640573.
49. Barat, R.; Bouzas, A.; Martí, N.; Ferrer, J.; Seco, A. Precipitation Assessment in Wastewater Treatment Plants Operated for Biological Nutrient Removal: A Case Study in Murcia, Spain. *J. Environ. Manag.* **2009**, *90*, 850–857. https://doi.org/10.1016/J.JENVMAN.2008.02.001.
50. Satoshi, Y.; Seichiro, O.; Hiroyuki, H.; Kotaro, A.; Mitoma, Y.; Hidetaka, K.; Biswas, B.K. Simultaneous Crystallization of Phosphate and Potassium as Magnesium Potassium Phosphate Using Bubble Column Reactor with Draught Tube. *J. Environ. Chem. Eng.* **2013**, *1*, 1154–1158. https://doi.org/10.1016/J.JECE.2013.08.032.
51. Chau, C.K.; Qiao, F.; Li, Z. Potentiometric Study of the Formation of Magnesium Potassium Phosphate Hexahydrate. *J. Mater. Civil. Eng.* **2012**, *24*, 586–591. https://doi.org/10.1061/(ASCE)MT.1943-5533.0000410.
52. Lahalle, H.; Coumes, C.C.D.; Mesbah, A.; Lambertin, D.; Cannes, C.; Delpech, S.; Gauffinet, S. Investigation of Magnesium Phosphate Cement Hydration in Diluted Suspension and Its Retardation by Boric Acid. *Cem. Concr. Res.* **2016**, *87*, 77–86. https://doi.org/10.1016/J.CEMCONRES.2016.04.010.
53. le Rouzic, M.; Chaussadent, T.; Platret, G.; Stefan, L. Mechanisms of K-Struvite Formation in Magnesium Phosphate Cements. *Cem. Concr. Res.* **2017**, *91*, 117–122. https://doi.org/10.1016/J.CEMCONRES.2016.11.008.
54. Lahalle, H.; Coumes, C.C.D.; Mercier, C.; Lambertin, D.; Cannes, C.; Delpech, S.; Gauffinet, S. Influence of the w/c Ratio on the Hydration Process of a Magnesium Phosphate Cement and on Its Retardation by Boric Acid. *Cem. Concr. Res.* **2018**, *109*, 159–174. https://doi.org/10.1016/J.CEMCONRES.2018.04.010.
55. Harada, H.; Katayama, Y.; Afriliana, A.; Inoue, M.; Teranaka, R.; Mitoma, Y. Effects of Co-Existing Ions on the Phosphorus Potassium Ratio of the Precipitate Formed in the Potassium Phosphate Crystallization Process. *J. Environ. Prot.* **2017**, *8*, 1424–1434. https://doi.org/10.4236/JEP.2017.811086.
56. Tarragó, E.; Ruscalleda, M.; Colprim, J.; Balaguer, M.D.; Puig, S. Towards a Methodology for Recovering K-Struvite from Manure. *J. Chem. Technol. Biotechnol.* **2018**, *93*, 1558–1562. https://doi.org/10.1002/JCTB.5518.
57. Warmadewanthi; Liu, J.C. Selective Precipitation of Phosphate from Semiconductor Wastewater. *J. Environ. Eng.* **2009**, *135*, 1063–1070. https://doi.org/10.1061/(ASCE)EE.1943-7870.0000054.
58. Taylor, A.W.; Frazier, A.W.; Gurney, E.L. Solubility Products of Magnesium Ammonium and Magnesium Potassium Phosphates. *Trans. Faraday Soc.* **1963**, *59*, 1580–1584. https://doi.org/10.1039/TF9635901580.
59. Huang, H.; Zhang, D.; Li, J.; Guo, G.; Tang, S. Phosphate Recovery from Swine Wastewater Using Plant Ash in Chemical Crystallization. *J. Clean. Prod.* **2017**, *168*, 338–345. https://doi.org/10.1016/J.JCLEPRO.2017.09.042.
60. Mamais, D.; Pitt, P.A.; Cheng, Y.W.; Loiacono, J.; Jenkins, D. Determination of Ferric Chloride Dose to Control Struvite Precipitation in Anaerobic Sludge Digesters. *Water Environ. Res.* **1994**, *66*, 912–918. https://doi.org/10.2175/WER.66.7.8.
61. Çelen, I.; Buchanan, J.R.; Burns, R.T.; Robinson, R.B.; Raman, D.R. Using a Chemical Equilibrium Model to Predict Amendments Required to Precipitate Phosphorus as Struvite in Liquid Swine Manure. *Water Res.* **2007**, *41*, 1689–1696. https://doi.org/10.1016/J.WATRES.2007.01.018.
62. Perwitasari, D.S.; Muryanto, S.; Tauviqirrahman, M.; Jamari, J.; Bayuseno, A.P. Optimization of Key Parameters in Struvite (K) Production for Phosphorus and Potassium Recovery Using a Batch Crystallizer. *Rasayan J. Chem.* **2019**, *12*, 787–795. https://doi.org/10.31788/RJC.2019.1225125.
63. Musvoto, E.V.; Wentzel, M.C.; Ekama, G.A. Integrated Chemical–Physical Processes Modelling—II. Simulating Aeration Treatment of Anaerobic Digester Supernatants. *Water Res.* **2000**, *34*, 1868–1880. https://doi.org/10.1016/S0043-1354(99)00335-8.
64. Musvoto, E. v; Ekama, G.A.; Wentzel, M.C.; Loewenthal, R.E. Extension and Application of the Three-Phase Weak Acid/Base Kinetic Model to the Aeration Treatment of Anaerobic Digester Liquors. *Water SA* **2000**, *26*, 417–438.
65. Wang, Y.; Mou, J.; Liu, X.; Chang, J. Phosphorus Recovery from Wastewater by Struvite in Response to Initial Nutrients Concentration and Nitrogen/Phosphorus Molar Ratio. *Sci. Total Environ.* **2021**, *789*, 147970. https://doi.org/10.1016/J.SCITOTENV.2021.147970.
66. Le Corre, K.S.; Valsami-Jones, E.; Hobbs, P.; Jefferson, B.; Parsons, S.A. Agglomeration of Struvite Crystals. *Water Res.* **2007**, *41*, 419–425. https://doi.org/10.1016/J.WATRES.2006.10.025.

67. Zhang, C.; Xu, K.N.; Li, J.Y.; Wang, C.W.; Zheng, M. Recovery of Phosphorus and Potassium from Source-Separated Urine Using a Fluidized Bed Reactor: Optimization Operation and Mechanism Modeling. *Ind. Eng. Chem. Res.* **2017**, *56*, 3033–3039. https://doi.org/10.1021/ACS.IECR.6B04819/ASSET/IMAGES/LARGE/IE-2016-048199_0006.JPEG.
68. Li, B.; Huang, H.M.; Boiarkina, I.; Yu, W.; Huang, Y.F.; Wang, G.Q.; Young, B.R. Phosphorus Recovery through Struvite Crystallisation: Recent Developments in the Understanding of Operational Factors. *J. Environ. Manag.* **2019**, *248*, 109254. https://doi.org/10.1016/J.JENVMAN.2019.07.025.
69. Kabdaşlı, I.; Tünay, O.; Udert K.M. Transfer into the solid phase. In *Source Separation and Decentralization for Wastewater Management*; Larsen, T.A., Udert, K.M., Lienert, J., Eds.; IWA Publishing: London, UK, 2013; pp. 351–365.
70. Kataki, S.; West, H.; Clarke, M.; Baruah, D.C. Phosphorus Recovery as Struvite: Recent Concerns for Use of Seed, Alternative Mg Source, Nitrogen Conservation and Fertilizer Potential. *Resour. Conserv. Recycl.* **2016**, *107*, 142–156. https://doi.org/10.1016/J.RESCONREC.2015.12.009.
71. Huang, H.; Li, J.; Li, B.; Zhang, D.; Zhao, N.; Tang, S. Comparison of Different K-Struvite Crystallization Processes for Simultaneous Potassium and Phosphate Recovery from Source-Separated Urine. *Sci. Total Environ.* **2019**, *651*, 787–795. https://doi.org/10.1016/J.SCITOTENV.2018.09.232.
72. Siciliano, A.; de Rosa, S. Recovery of Ammonia in Digestates of Calf Manure through a Struvite Precipitation Process Using Unconventional Reagents. *Environ. Technol.* **2014**, *35*, 841–850. https://doi.org/10.1080/09593330.2013.853088.
73. Siciliano, A.; Ruggiero, C.; de Rosa, S. A New Integrated Treatment for the Reduction of Organic and Nitrogen Loads in Methanogenic Landfill Leachates. *Process. Saf. Environ. Prot.* **2013**, *91*, 311–320. https://doi.org/10.1016/J.PSEP.2012.06.008.
74. Zhang, C.; Chen, Y. Simultaneous Nitrogen and Phosphorus Recovery from Sludge-Fermentation Liquid Mixture and Application of the Fermentation Liquid to Enhance Municipal Wastewater Biological Nutrient Removal. *Environ. Sci. Technol.* **2009**, *43*, 6164–6170. https://doi.org/10.1021/ES9005948/SUPPL_FILE/ES9005948_SI_001.PDF.
75. Xu, K.; Zhang, C.; Li, J.; Cheng, X.; Wang, C. Removal and Recovery of N, P and K from Urine via Ammonia Stripping and Precipitations of Struvite and Struvite-K. *Water Sci. Technol.* **2017**, *75*, 155–164. https://doi.org/10.2166/WST.2016.494.
76. Lee, S.H.; Yoo, B.H.; Lim, S.J.; Kim, T.H.; Kim, S.K.; Kim, J.Y. Development and Validation of an Equilibrium Model for Struvite Formation with Calcium Co-Precipitation. *J. Cryst. Growth* **2013**, *372*, 129–137. https://doi.org/10.1016/J.JCRYSGRO.2013.03.010.
77. Yan, H.; Shih, K. Effects of Calcium and Ferric Ions on Struvite Precipitation: A New Assessment Based on Quantitative X-Ray Diffraction Analysis. *Water Res.* **2016**, *95*, 310–318. https://doi.org/10.1016/J.WATRES.2016.03.032.
78. Abbona, F.; Madsen, H.E.L.; Boistelle, R. The Initial Phases of Calcium and Magnesium Phosphates Precipitated from Solutions of High to Medium Concentrations. *J. Cryst. Growth* **1986**, *74*, 581–590. https://doi.org/10.1016/0022-0248(86)90205-8.
79. Abbona, F.; Lundager Madsen, H.E.; Boistelle, R. The Final Phases of Calcium and Magnesium Phosphates Precipitated from Solutions of High to Medium Concentration. *J. Cryst. Growth* **1988**, *89*, 592–602. https://doi.org/10.1016/0022-0248(88)90223-0.
80. Abbona, F.; Franchini-Angela, M.; Boistelle, R. Crystallization of Calcium and Magnesium Phosphates from Solutions of Medium and Low Concentrations. *Cryst. Res. Technol.* **1992**, *27*, 41–48. https://doi.org/10.1002/CRAT.2170270107.
81. Li, B.; Boiarkina, I.; Yu, W.; Young, B. A New Thermodynamic Approach for Struvite Product Quality Prediction. *Environ. Sci. Pollut. Res.* **2019**, *26*, 3954–3964. https://doi.org/10.1007/S11356-018-3889-7/TABLES/6.
82. Capdevielle, A.; Sýkorová, E.; Béline, F.; Daumer, M.L. Kinetics of Struvite Precipitation in Synthetic Biologically Treated Swine Wastewaters. *Environ. Technol.* **2014**, *35*, 1250–1262. https://doi.org/10.1080/09593330.2013.865790.
83. Liu, X.; Wang, J. Impact of Calcium on Struvite Crystallization in the Wastewater and Its Competition with Magnesium. *Chem. Eng. J.* ***2019***, *378*, 122121. https://doi.org/10.1016/J.CEJ.2019.122121.
84. Enyemadze, I.; Momade, F.W.Y.; Oduro-Kwarteng, S.; Essandoh, H. Phosphorus Recovery by Struvite Precipitation: A Review of the Impact of Calcium on Struvite Quality. *J. Water Sanit. Hyg. Dev.* **2021**, *11*, 706–718. https://doi.org/10.2166/WASHDEV.2021.078.
85. Yang, H.; Sun, H.J. Crystal Structure of a New Phosphate Compound, $Mg_2KNa(PO_4)_2{\cdot}14H_2O$. *J. Solid State Chem.* **2004**, *177*, 2991–2997. https://doi.org/10.1016/J.JSSC.2004.05.008.
86. Tansel, B.; Lunn, G.; Monje, O. Struvite Formation and Decomposition Characteristics for Ammonia and Phosphorus Recovery: A Review of Magnesium-Ammonia-Phosphate Interactions. *Chemosphere* **2018**, *194*, 504–514. https://doi.org/10.1016/J.CHEMOSPHERE.2017.12.004.
87. Ghosh, S.; Lobanov, S.; Lo, V.K. An Overview of Technologies to Recover Phosphorus as Struvite from Wastewater: Advantages and Shortcomings. *Environ. Sci. Pollut. Res.* **2019**, *26*, 19063–19077. https://doi.org/10.1007/S11356-019-05378-6.
88. Zhang, C.; Xu, K.; Zheng, M.; Li, J.; Wang, C. Factors Affecting the Crystal Size of Struvite-K Formed in Synthetic Urine Using a Stirred Reactor. *Ind. Eng. Chem. Res.* **2018**, *57*, 17301–17309. https://doi.org/10.1021/ACS.IECR.8B03328/ASSET/IMAGES/LARGE/IE-2018-03328A_0006.JPEG.
89. Yilmazel, Y.D.; Demirer, G.N. Removal and Recovery of Nutrients as Struvite from Anaerobic Digestion Residues of Poultry Manure. *Environ. Technol.* **2011**, *32*, 783–794. https://doi.org/10.1080/09593330.2010.512925.
90. Rech, I.; Kamogawa, M.Y.; Jones, D.L.; Pavinato, P.S. Synthesis and Characterization of Struvite Derived from Poultry Manure as a Mineral Fertilizer. *J. Environ. Manag.* **2020**, *272*, 111072. https://doi.org/10.1016/J.JENVMAN.2020.111072.
91. Atalay, S.; Sargin, I.; Arslan, G. Crystallization of Struvite-K from Pumpkin Wastes. *J. Sci. Food Agric.* **2022**, *102*, 523–530. https://doi.org/10.1002/JSFA.11380.
92. Monfet, E.; Aubry, G.; Ramirez, A.A. Nutrient Removal and Recovery from Digestate: A Review of the Technology. *Biofuels* **2018**, *9*, 247–262. https://doi.org/10.1080/17597269.2017.1336348.

93. Tao, W.; Fattah, K.P.; Huchzermeier, M.P. Struvite Recovery from Anaerobically Digested Dairy Manure: A Review of Application Potential and Hindrances. *J. Environ. Manag.* **2016**, *169*, 46–57. https://doi.org/10.1016/J.JENVMAN.2015.12.006.
94. Kim, D.; Min, K.J.; Lee, K.; Yu, M.S.; Park, K.Y. Effects of PH, Molar Ratios and Pre-Treatment on Phosphorus Recovery through Struvite Crystallization from Effluent of Anaerobically Digested Swine Wastewater. *Environ. Eng. Res.* **2017**, *22*, 12–18. https://doi.org/10.4491/EER.2016.037.
95. Zeng, L.; Li, X. Nutrient Removal from Anaerobically Digested Cattle Manure by Struvite Precipitation. *J. Environ. Eng. Sci.* **2015**, *5*, 285–294. https://doi.org/10.1139/S05-027.
96. Gorazda, K.; Tarko, B.; Werle, S.; Wzorek, Z. Sewage Sludge as a Fuel and Raw Material for Phosphorus Recovery: Combined Process of Gasification and P Extraction. *Waste Manag.* **2018**, *73*, 404–415. https://doi.org/10.1016/J.WASMAN.2017.10.032.
97. Acelas, N.Y.; López, D.P.; Wim Brilman, D.W.F.; Kersten, S.R.A.; Kootstra, A.M.J. Supercritical Water Gasification of Sewage Sludge: Gas Production and Phosphorus Recovery. *Bioresour. Technol.* **2014**, *174*, 167–175. https://doi.org/10.1016/J.BIORTECH.2014.10.003.
98. Atoufi, H.D.; Lampert, D.J. Impacts of Oil and Gas Production on Contaminant Levels in Sediments. *Curr. Pollut. Rep.* **2020**, *6*, 43–53. https://doi.org/10.1007/S40726-020-00137-5/TABLES/2.
99. Hu, L.; Yu, J.; Luo, H.; Wang, H.; Xu, P.; Zhang, Y. Simultaneous Recovery of Ammonium, Potassium and Magnesium from Produced Water by Struvite Precipitation. *Chem. Eng. J.* **2020**, *382*, 123001. https://doi.org/10.1016/J.CEJ.2019.123001.
100. Li, X.; Zhu, W.; Wu, Y.; Wang, C.; Zheng, J.; Xu, K.; Li, J. Recovery of Potassium from Landfill Leachate Concentrates Using a Combination of Cation-Exchange Membrane Electrolysis and Magnesium Potassium Phosphate Crystallization. *Sep. Purif. Technol.* **2015**, *144*, 1–7. https://doi.org/10.1016/J.SEPPUR.2015.01.035.
101. Wu, S.; Zou, S.; Liang, G.; Qian, G.; He, Z. Enhancing Recovery of Magnesium as Struvite from Landfill Leachate by Pretreatment of Calcium with Simultaneous Reduction of Liquid Volume via Forward Osmosis. *Sci. Total Environ.* **2018**, *610–611*, 137–146. https://doi.org/10.1016/J.SCITOTENV.2017.08.038.
102. Gaterell, M.R.; Gay, R.; Wilson, R.; Gochin, R.J.; Lester, J.N. An Economic and Environmental Evaluation of the Opportunities for Substituting Phosphorus Recovered from Wastewater Treatment Works in Existing UK Fertiliser Markets. *Environ. Technol.* **2011**, *21*, 1067–1084. https://doi.org/10.1080/09593332108618050.
103. Dunseth, M.G.; Salutsky, M.L.; Ries, K.M.; Shapiro, J.J. *Ultimate Disposal of Phosphates from Wastewater by Recovery as Fertilizer*; Water Pollution Control Research Series, 17070ESJ 01/70; US Department of the Interior; Federal Water Quality Administration: Washington, DC, USA, 1970.
104. El Diwani, G.; El Rafie, S.; El Ibiari, N.N.; El-Aila, H.I. Recovery of Ammonia Nitrogen from Industrial Wastewater Treatment as Struvite Slow Releasing Fertilizer. *Desalination* **2007**, *214*, 200–214. https://doi.org/10.1016/J.DESAL.2006.08.019.
105. Ryu, H.D.; Lim, C.S.; Kang, M.K.; Lee, S.I. Evaluation of Struvite Obtained from Semiconductor Wastewater as a Fertilizer in Cultivating Chinese Cabbage. *J. Hazard. Mater.* **2012**, *221–222*, 248–255. https://doi.org/10.1016/J.JHAZMAT.2012.04.038.
106. Uysal, A.; Yilmazel, Y.D.; Demirer, G.N. The Determination of Fertilizer Quality of the Formed Struvite from Effluent of a Sewage Sludge Anaerobic Digester. *J. Hazard. Mater.* **2010**, *181*, 248–254. https://doi.org/10.1016/J.JHAZMAT.2010.05.004.
107. Uysal, A.; Demir, S.; Sayilgan, E.; Eraslan, F.; Kucukyumuk, Z. Optimization of Struvite Fertilizer Formation from Baker's Yeast Wastewater: Growth and Nutrition of Maize and Tomato Plants. *Environ. Sci. Pollut. Res.* **2014**, *21*, 3264–3274. https://doi.org/10.1007/S11356-013-2285-6.
108. Siciliano, A. Assessment of Fertilizer Potential of the Struvite Produced from the Treatment of Methanogenic Landfill Leachate Using Low-Cost Reagents. *Environ. Sci. Pollut. Res.* **2016**, *23*, 5949–5959. https://doi.org/10.1007/S11356-015-5846-Z/TABLES/11.
109. Liu, Y.H.; Rahman, M.M.; Kwag, J.-H.; Kim, J.-H.; Ra, C.S. Eco-Friendly Production of Maize Using Struvite Recovered from Swine Wastewater as a Sustainable Fertilizer Source. *Asian-Australas. J. Anim. Sci.* **2011**, *24*, 1699–1705. https://doi.org/10.5713/AJAS.2011.11107.
110. El-Nakhel, C.; Geelen, D.; de Paepe, J.; Clauwaert, P.; de Pascale, S.; Rouphael, Y. An Appraisal of Urine Derivatives Integrated in the Nitrogen and Phosphorus Inputs of a Lettuce Soilless Cultivation System. *Sustainability* **2021**, *13*, 4218. https://doi.org/10.3390/SU13084218.
111. Regulation (EU) 2019/1009 of the European Parliament and of the Council of 5 June 2019 Laying down Rules on the Making Available on the Market of EU Fertilising Products and Amending Regulations (EC) No. 1069/2009 and (EC) No. 1107/2009 and Repealing Regulation (EC) No. 2003/2003. Available online: https://eur-lex.europa.eu/legal-content/EN/TXT/?uri=celex%3A32019R1009 (accessed on 22 July 2022).